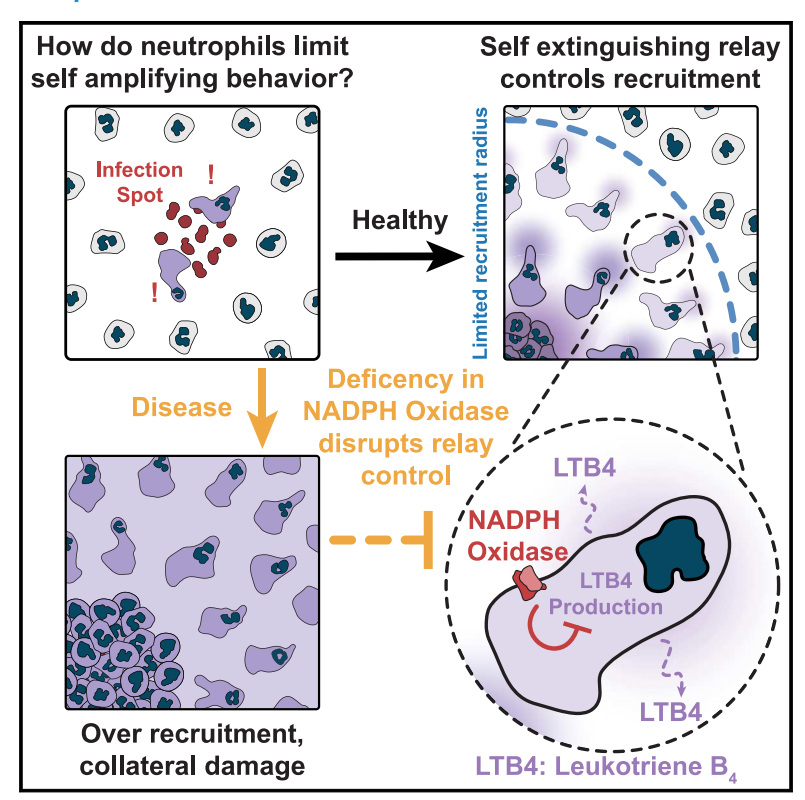
Self-extinguishing relay waves enable homeostatic control of human neutrophil swarming

Graphical abstract



Authors

Evelyn Strickland, Deng Pan, Christian Godfrey, ..., Daniel Irimia, Ariel Amir, Orion D. Weiner

Correspondence

orion.weiner@ucsf.edu

In brief

Strickland et al. find that human neutrophils organize pulsatile, self-extinguishing waves of leukotriene B4 to ensure robust homeostatic recruitment. Self-extinguishing waves are dependent on the activity of NADPH oxidase, and deficiency in this pathway leads to a reduced ability to extinguish relay waves.

Highlights

- Neutrophil swarming is organized by pulsatile, selfextinguishing waves of LTB4
- NADPH-oxidase activation is critical for relay wave selfextinction
- Neutrophils adjust the size and number of waves to homeostatically control recruitment
- Chronic granulomatosis disease neutrophils generate undamped relay waves that do not extinguish



Developmental Cell



Article

Self-extinguishing relay waves enable homeostatic control of human neutrophil swarming

Evelyn Strickland,^{1,2} Deng Pan,³ Christian Godfrey,^{4,5} Julia S. Kim,¹ Alex Hopke,^{4,5,6} Wencheng Ji,⁷ Maureen Degrange,⁸ Bryant Villavicencio,⁹ Michael K. Mansour,^{5,10} Christa S. Zerbe,¹¹ Daniel Irimia,^{4,5,6} Ariel Amir,^{3,7} and Orion D. Weiner^{1,2,12,*}

¹Department of Biochemistry and Biophysics, University of California, San Francisco, San Francisco, CA, USA

SUMMARY

Neutrophils collectively migrate to sites of injury and infection. How these swarms are coordinated to ensure the proper level of recruitment is unknown. Using an *ex vivo* model of infection, we show that human neutrophil swarming is organized by multiple pulsatile chemoattractant waves. These waves propagate through active relay in which stimulated neutrophils trigger their neighbors to release additional swarming cues. Unlike canonical active relays, we find these waves to be self-terminating, limiting the spatial range of cell recruitment. We identify an NADPH-oxidase-based negative feedback loop that is needed for this self-terminating behavior. We observe near-constant levels of neutrophil recruitment over a wide range of starting conditions, revealing surprising robustness in the swarming process. This homeostatic control is achieved by larger and more numerous swarming waves at lower cell densities. We link defective wave termination to a broken recruitment homeostat in the context of human chronic granulomatous disease.

INTRODUCTION

During collective migration, individual organisms coordinate their movement to solve critical tasks. Birds flock, fish school, and insects swarm to escape predation, find food, and navigate complex environments efficiently. These organismal collectives rely on individuals acting on local information, such as external environmental cues, neighbor behaviors, or self-generated chemical cues, to create complex emergent decisions. Collective migration is also organized at the cellular level, where groups of cells coordinate wound healing, Scancer metastasis, multicellular morphogenesis, and the transition from single-cell to multicellular existence. Although some examples of collective cell migration are well understood, such as *Dictyostelium* aggregation, Series as comparable understanding of the collective rules that organize the human immune response.

Neutrophils are first responders of the innate immune system that are recruited to sites of injury and infection to neutralize invading pathogens and aid in tissue repair. 14-16 Because the

primary signals of injury/infection are relatively short-ranged, activated neutrophils release chemoattractants such as leukotriene B4 (LTB₄) that act to augment the recruitment of additional neutrophils. This self-amplified "swarming" process significantly enhances the speed and range of recruitment, ^{17–21} but this process must be tightly regulated to limit collateral damage. ^{17,22–24} Although some brakes on swarming are known, ^{17,20,22} how neutrophils control the spatiotemporal dynamics of cell-cell communication to recruit the appropriate number of cells early in the swarming process is not well understood.

Although many neutrophil swarming studies have been performed in living animals, ^{17,19,21,22,25-28} the *in vivo* context presents several challenges for mechanistic dissection of the swarming process. For example, multiple cell types modulate swarm initiation and propagation, ²² there are a multitude of diffusive signals following tissue damage, ^{21,22} and the *in vivo* migration environment is complex and difficult to image at high spatiotemporal resolution. These challenges make it difficult to mechanistically dissect the regulation of swarming.

²Cardiovascular Research Institute, University of California, San Francisco, San Francisco, CA, USA

³John A. Paulson School of Engineering and Applied Sciences, Harvard University, Cambridge, MA, USA

⁴Center for Engineering in Medicine and Surgery, Department of Surgery, Massachusetts General Hospital, Boston, MA, USA

⁵Harvard Medical School, Boston, MA, USA

⁶Shriners Burns Hospital, Boston, MA 02114, USA

⁷Department of Physics of Complex Systems, The Weizmann Institute of Science, Rehovot 7610001, Israel

⁸Leidos Biomedical Research, Inc., Frederick National Laboratory for Cancer Research, Frederick, MD 21702, USA

⁹Kelly Government Services, Bethesda, MD, USA

¹⁰Division of Infectious Diseases, Massachusetts General Hospital, Boston, MA, USA

¹¹Laboratory of Clinical Immunology and Microbiology (LCIM), National Institute of Allergy and Infectious Diseases (NIAID), National Institutes of Health (NIH), Bethesda, MD, USA

¹²Lead contact

^{*}Correspondence: orion.weiner@ucsf.edu https://doi.org/10.1016/j.devcel.2024.06.003



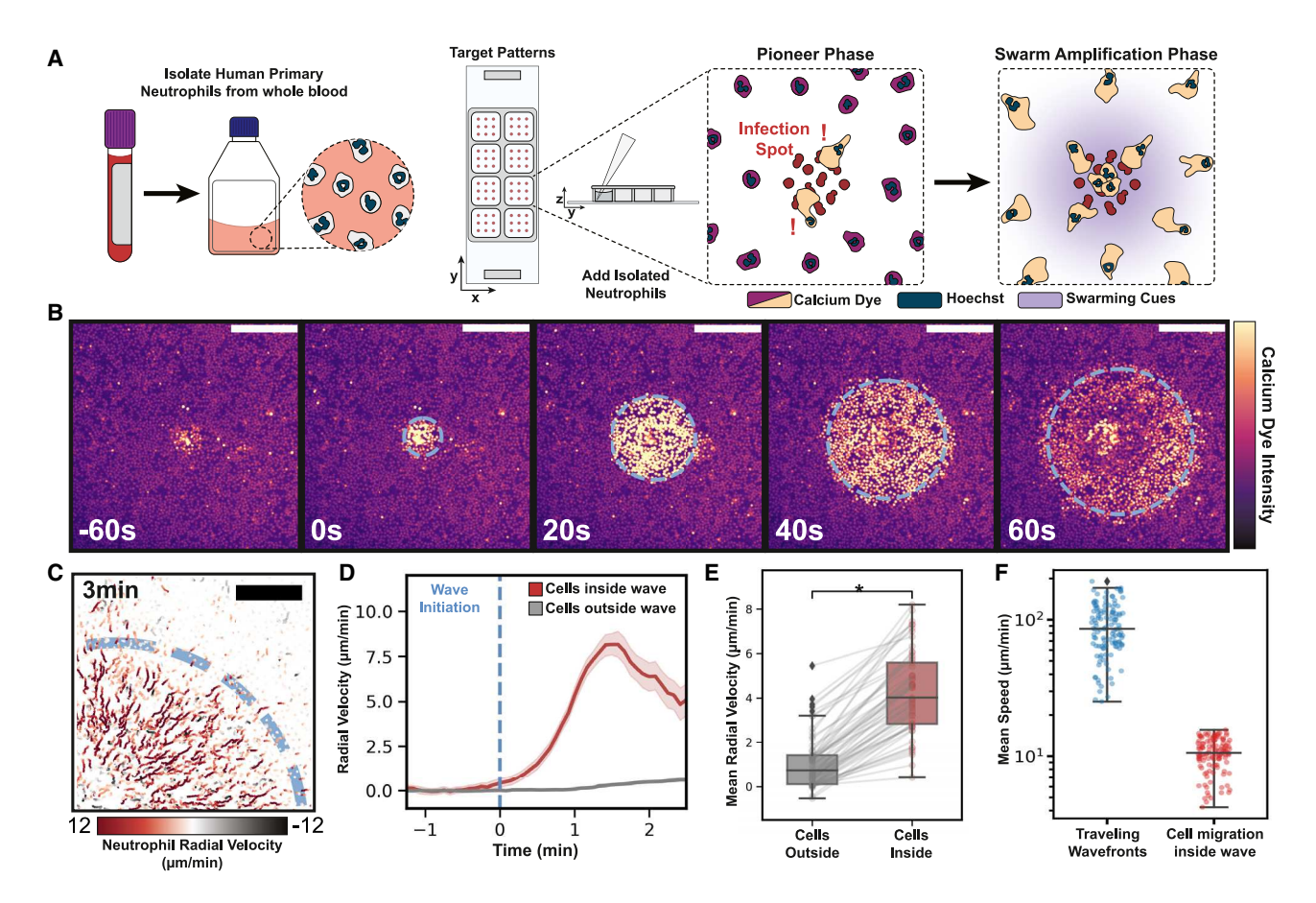


Figure 1. Fast-moving multicellular signaling waves define the zone of recruitment in human neutrophil swarming

(A) Ex vivo assay for neutrophil swarming with self-amplified recruitment of cells in response to local site of heat-killed Candida albicans. Human neutrophils are isolated via immunomagnetic selection and dyed with CalBryte 520-AM (cytosolic Ca²⁺ reporter, used to monitor neutrophil detection of pathogen and swarming cues) and Hoechst 3334 (nuclear marker, used to track cell movement). Cells are placed on printed targets of heat-killed Candida albicans, and neutrophil swarming responses are monitored via confocal microscopy.

- (B) Time-lapse sequence of a multicellular wave of neutrophil Ca^{2+} activity following detection of the fungal target. The dotted line represents the wave boundary, as tracked by our analysis software; scale bars, 200 μm .
- (C) The signaling wave defines the zone of neutrophil recruitment toward the fungal target. The blue dashed line denotes the final radius of the wave shown in (B). Cell tracks for 3 min following wave initiation are indicated with color corresponding to radial velocity toward the wave center; scale bars, 100 µm.
- (D) Average radial velocity for cells inside versus outside the final wave boundary is plotted over 6 min for a population of cells during a single wave event (Average shown with 95% confidence interval shaded; cell tracks inside the wave n = 3,720, outside wave tracks n = 9,499). Wave boundary predicts zone of recruitment during swarming.
- (E) Comparison of mean radial velocity for cells inside versus outside the largest wave boundary in each experiment. Tracks were averaged over the duration of the wave event, and lines connect mean radial velocities of outer versus inner cells for each experiment. Dependent paired t test p value = 5.8×10^{-27} ; target ROIs n = 56. (F) Average velocity of the signaling waves propagated across the field of cells during swarming compared with the average cell velocity for the cells within these wave boundaries. Signaling waves are approximately 1 order of magnitude faster than cell movement during swarming.

Furthermore, a focus on model organisms precludes the analysis of swarming for human neutrophils despite known differences in primary human neutrophil behaviors compared with model systems. To address these limitations, we leverage an *ex vivo* assay to study human neutrophil swarming in response to controllable, reproducible, and well-defined cues. This assay expands upon our previously developed *ex vivo* swarming system^{20,31} in which a defined grid of heat-killed *Candida albicans* "targets" are spotted on a thin slip of glass to act as an array of swarm initiation sites. Healthy human primary neutrophils isolated from whole blood are added to the assay, and swarming responses centered on the targets are observed with live cell microscopy.

RESULTS

Fast-moving multicellular signaling waves define the zone of recruitment in human neutrophil swarming

To monitor cell-cell communication in conjunction with more traditional swarming readouts like motility, we used a cytosolic calcium dye. Neutrophils increase cytosolic calcium following exposure to primary chemoattractants and swarming cues such as LTB₄,³² and we envisioned that monitoring calcium influx would enable us to follow the propagation of swarming signals and correlate these to the regulation of directed cell movement (Figure 1A). Furthermore, calcium signals at the core of injury sites *in vivo* have been linked to key swarm signaling

Article



events, ¹⁹ and the simpler planar geometry along with the higher signal-to-noise imaging of our assay should enable a more sensitive detection of swarm signal propagation to neutrophils far from the heat-killed *Candida albicans* target. Although calcium signaling has been studied during mice and zebrafish swarming, ^{19,27} it has not during human neutrophil swarming, and a lack of quantitative tools for analyzing cell-cell communication has limited a deeper mechanistic dissection of the swarming process using this readout.

Following neutrophil introduction to the assay, we observe a calcium influx of the neutrophils that are in contact with the fungal target as well as multiple multicellular waves of calcium activity that radially propagate away from the target to surrounding neutrophils (Video S1). An example time course of these waves is shown in Figure 1B, with the overlaid tracked boundary of the wave. Wave tracks are calculated by fitting a circle to a cloud of cells that are determined to be active via calcium signal binning and grouped using the ARCOS algorithm³³ (Figures S1A and S1B; Video S1). Wave movement is roughly isotropic, and the fitting of waves to a circle enables the tracking of wave propagation kinetics (Figures S1C and S1D). Immediately following the passage of a signaling wave, cells rapidly polarize and migrate radially toward the wave origin site. Cells within the wave perimeter move toward the fungal target, while cells outside the wave perimeter lack coordinated movement (Figures 1C and 1D). By analyzing cell responses across many targets and donors, we observe that most, if not all, movement occurs within the boundaries of tracked signaling waves, indicating that these wavefronts represent an effective boundary of the swarming guidance cue reception (Figure 1E). Though the propagating waves delimit the zone of recruited neutrophils, they operate at very different timescales with respect to neutrophil movement. Signaling waves move an order of magnitude faster than the resulting neutrophil chemotaxis toward the wave origin (Figure 1F) and propagate in the opposite direction to cell movement during swarming. The dramatically different timescales of wave propagation and cell movement suggest that the movement of neutrophils does not play a significant role in the propagation of individual swarming waves.

Signaling waves are mediated by LTB₄ and are consistent with active relay, but not core production models

LTB₄, an inflammatory lipid of the leukotriene family, is thought to be one of the key secreted molecules that regulates neutrophil swarming. ^{20,21} Neutrophils release LTB₄ in response to various damage-associated pattern molecules and pathogen-associated pattern molecules, ^{20,34,35} including *Candida albicans*. ³⁶ To test whether LTB₄ reception is required for the rapid long-range waves in our *ex vivo* swarming assay, we blocked LTB₄ reception with the LTB₄ receptor antagonist BIIL315. ³⁷ Blocking LTB₄ receptors inhibited the rapidly propagating long-range signaling waves that accompany swarming. In the absence of LTB₄ reception, a much smaller-range, slow-moving signaling wave was observed (Figures S2B and S2C; Video S2). Quantitative analysis of wave propagation in both settings indicates that the rapid, long-range signaling waves that accompany swarming are dependent on LTB₄ reception (Figure 2A).

We next investigated how the LTB₄ ligands are propagated from the target site to the rest of the field. Two models have been proposed for the signal amplification observed during swarming. For the relay model of swarming, pioneer neutrophils at the site of infection secrete LTB₄, which activates surrounding neutrophils to synthesize and secrete additional LTB4 and LTB4 precursors, thereby continuing the relay. 21,34,35,38-43 This active relay mechanism could enable neutrophils to collectively signal across significant distances from the injury/infection site, analogous to cell-cell signal propagation in aggregating Dictyostelium. 44,45 In contrast, for the core production model of swarming, only neutrophils in direct contact with the site of injury/infection produce significant LTB4, which then passively diffuses into the tissue to attract more neutrophils. 19 These two swarming models give very different predictions for the dynamics of propagation of the LTB4 wavefront as it moves away from the site of infection. The relay model predicts a wave that travels at a fixed velocity because of continuous signal re-amplification at the traveling front. This produces an activation zone whose area (wave-fit circle radius squared [R²]) scales quadratically in time. In contrast, because the core diffusion model predicts LTB₄ production restricted to a central source, this system is limited by diffusion and, therefore, its activation area (R2) scales linearly in time (Figure 2B).

Using this framework, we tracked the radius squared versus time for multiple waves across many healthy donors in control cells (Figure 2C) versus LTB₄-blockaded neutrophils (Figure 2D) and fit a power law to each individual wave trajectory. This analysis reveals that control cells exhibit an LTB4 reception-dependent wave propagation with an alpha close to 2, consistent with the active relay model of swarming and inconsistent with the core production model of swarming (Figure 2E). Furthermore, upon fitting our observations to basic models of active relay and diffusion from a central source alone, 38 we find that the convex shape of the relay model best matches our early-wave kinetics, further supporting relay as the mechanism of signal propagation (Figure 2F). In the absence of LTB₄ signal reception, cells exhibit a slower, shorter-range pattern of signal propagation with an alpha close to 1 (Figure 2E), consistent with core diffusion alone. These data suggest that the residual release of non-LTB4 swarming ligands, such as interleukin-8 (IL-8),20 from cells on the target create a shallow, diffusive gradient with limited chemoattraction (Figure S2C). These residual waves are best fit with a central diffusive model and have a radius squared relation to time that appears linear (Figure 2G). These two examples establish that we can distinguish between diffusive waves and relay-mediated ones and that LTB4-receptor-mediated waves exhibit relay-like, ballistic spreading in the early phase of wave propagation.

Swarming relay waves self-extinguish through an NADPH-oxidase-based negative feedback mechanism

Our observation that neutrophil swarming cues radiate from heat-killed yeast targets via active relay might be expected to produce waves that continue to propagate as long as there are nearby receptive cells to continue the wave. This is the behavior of actively relayed systems, including action potentials, mitotic waves, and *Dictyostelium* aggregation. We previously proposed an active relay model for swarming in which cells that



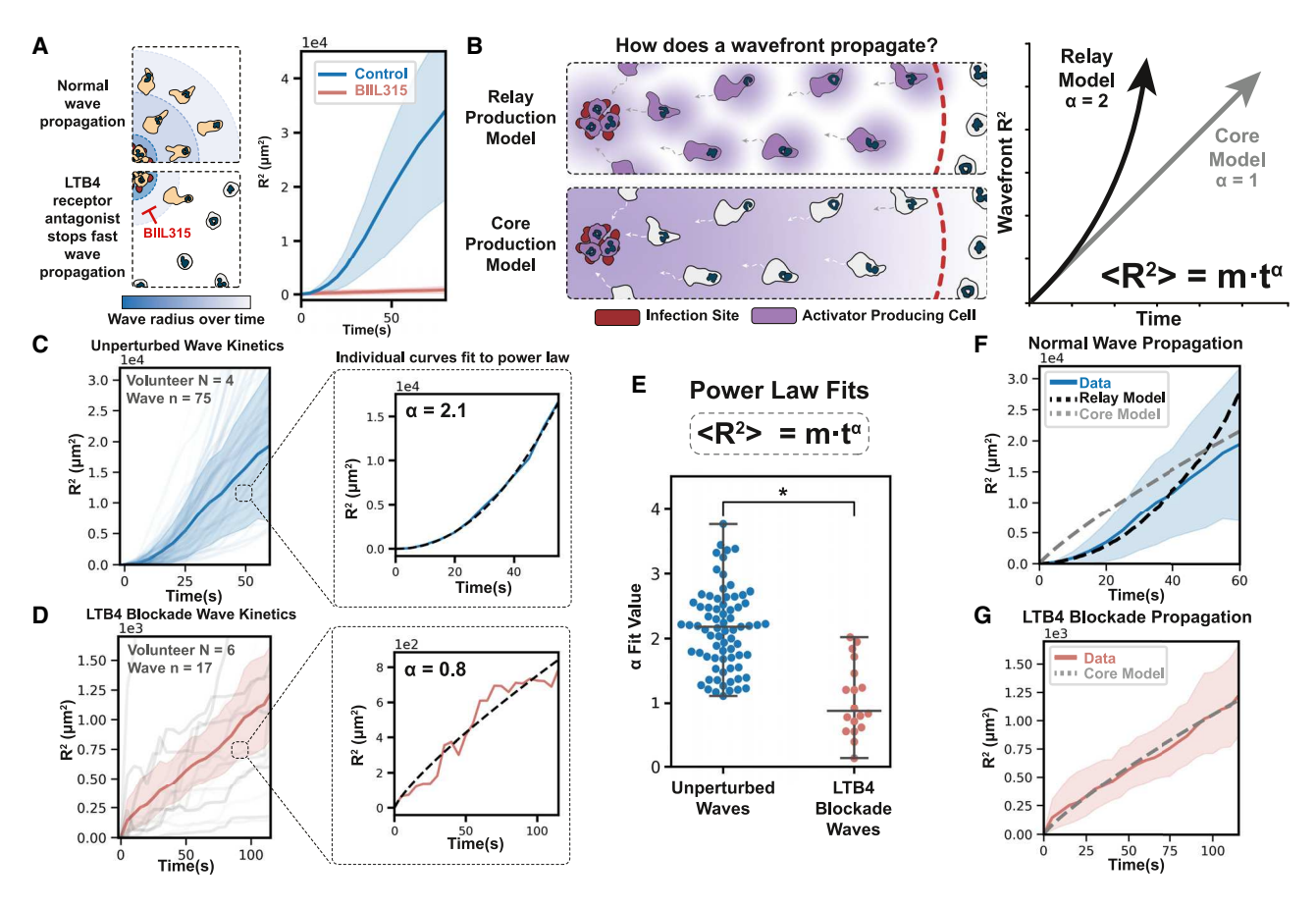


Figure 2. Signaling waves are mediated by LTB₄ and are consistent with active relay but not core production models

(A) Signal propagation across a field of neutrophils during swarming for cells in the absence (50 waves) or presence (17 waves) of an LTB₄ receptor inhibitor (1 μM BIIL315); averages shown with 95% confidence interval shaded. LTB₄ reception is required for rapid, long-range wave propagation.

- (B) Two proposed models of LTB₄ propagation from a site of infection to the rest of the field with the predicted kinetics of signal propagation shown for each. In a relay model of swarming, ^{21,34,38} each activated neutrophil releases LTB₄, which stimulates the adjacent cell to release LTB₄; this wave should spread with a constant velocity over time, giving an alpha of 2. For a core production model of swarming, ¹⁹ only neutrophils at the center of a swarm produce LTB₄, which moves across the field through passive diffusion; this wave should spread with an alpha of 1 (linear on R² plot).
- (C) Average early-wave kinetics for control cells with mean and 95% confidence interval. Individual tracks are fit to a power law equation to determine the alpha of wave propagation for each experiment.
- (D) Wave propagation for LTB4R-inhibited cells averaged with 95% confidence interval are individually fit to a power law equation for the first 2 min following swarm initiation.
- (E) Resulting curve fit alpha parameters for both unperturbed and LTB4R blockade conditions are plotted, with control cells showing wave propagation consistent with active relay. LTB₄ reception-inhibited cells showed residual wave propagation consistent with core diffusion. Welch's t test p value = 4.0×10^{-8} .
- (F) Same data as (C), replotted and fit to a simple relay model.³⁸ For the core diffusion model to match the final radius mean at 60 s, its early kinetics must outpace the experimental data, allowing us to exclude core production as the dominant mechanism of wave propagation. In contrast, our experimental data are consistent with active relay.
- (G) Same data as (D), replotted and fit to the core model. The shape of the model curve gives a good agreement with our data in this case, indicating that following LTB₄ receptor blockade, residual swarm cues diffuse away from a central source by passive diffusion and not active relay.

pass a threshold amount of LTB₄ themselves create more LTB₄, as shown in Figure 3A.³⁸ Once initiated, these waves continue to propagate indefinitely, given a field of responsive cells. In contrast with the predictions of a simple relay model, our experimentally observed waves propagate and then abruptly stop (Figures 3B and 3C), indicating a more complex mode of regulation than positive feedback alone.

Because there are multiple circuits that negatively regulate the production of LTB $_4$, $^{47-50}$ we envisioned that one of these negative feedback circuits could collaborate with LTB $_4$ -positive feedback to enable self-termination of neutrophil swarming waves.

What might serve as the activation-dependent inhibitor in this self-extinguishing relay mechanism? The inhibitor should be activated downstream of LTB₄ reception, and the effect of this inhibitor should attenuate LTB₄ production. NADPH oxidase activation satisfies both conditions. NADPH oxidase is used in ROS-dependent pathogen killing downstream of LTB₄, ^{31,47,51} and the inhibition of NADPH oxidase activation potentiates LTB₄ production and neutrophil accumulation during swarming. ^{31,47,52–54} If NADPH oxidase activity is a critical component in self-extinguishing relay, we would expect NADPH oxidase inhibition to prevent swarming wave termination, thereby enabling

Article



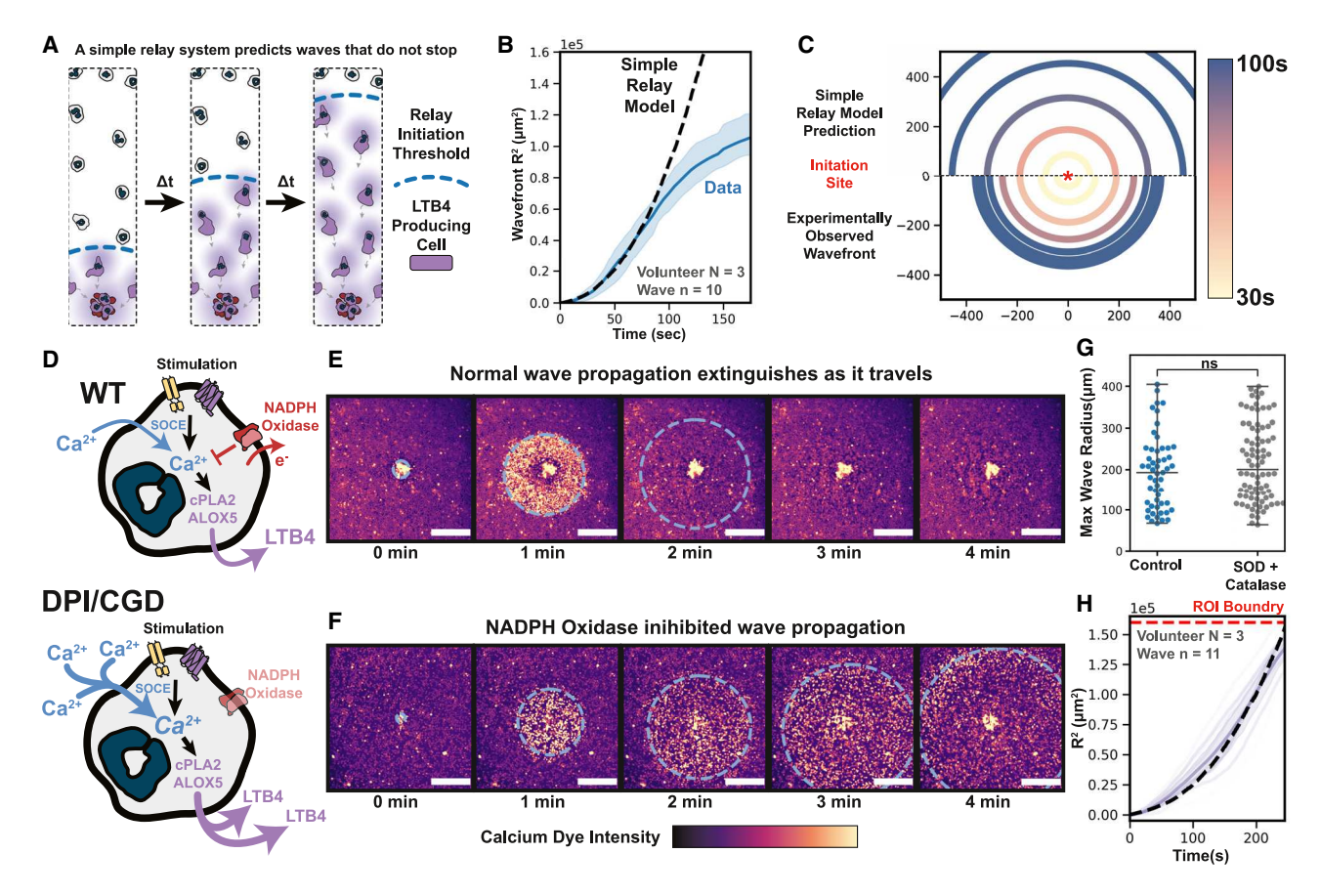


Figure 3. Swarming relay waves self-extinguish through an NADPH-oxidase-based negative feedback mechanism

(A) Our previously proposed simple diffusive relay model of swarming.³⁸ As cells exceed a threshold amount of extracellular LTB4, they begin to release more LTB4 to their surroundings, thereby activating adjacent cells to continue the relay. This wave propagates indefinitely once initiated in a homogenous field of cells. (B) Although experimental waves initially propagate with a relay-like R² relation, in the latter phase the waves decelerate then stop. Average radial kinetics of 10 large waves with similar termination distances shown with the 95% confidence interval shaded.

(C) Comparing the simple diffusive relay prediction with an average of experimentally observed swarming wavefronts shows how wave behavior diverges from experiment. Experimental relay waves come to a stop (bottom), whereas simple relay propagates indefinitely (top); axes in μ m; wave n = 5. Volunteer N = 2. (D) NADPH oxidase activation normally limits calcium influx, which, in turn, reduces LTB4 production.⁴⁷ Inhibition of NADPH oxidase activation removes this brake on calcium influx and LTB4 production.

(E) Time-lapse sequence of a representative signaling wave for unperturbed neutrophils. Dotted line represents tracked wave boundary. Boundary line is removed when the wave terminates and dissipates; scale bars, 200 µm.

(F) Time-lapse sequence of a representative signaling wave for cells treated with NADPH oxidase inhibitor (50 μ M of DPI for 15 min) before seeding in assay. Dotted line represents tracked wave boundary that, unlike control cells, continues to propagate beyond the field of view (\sim 400 μ m from target); scale bars, 200 μ m.

(G) Sequestration of extracellular ROS through addition of human SOD (200 U/mL) and human catalase (>200 U/mL) to the swarming assay does not appreciably change wave termination behaviors. In conjunction with the DPI experiments, our work supports the role of cell-intrinsic activation of NADPH oxidase for wave termination. Wave n = 137, volunteer N = 3. Welch's t test p value = 0.16, ns.

(H) Inhibition of NADPH oxidase activity via the NADPH oxidase inhibitor DPI (50 μ M) produces swarming waves that no longer stop in the observable microscopic field and mimic simple relay dynamics throughout their propagation (volunteer N=3, wave n=11). Average plotted with 95% cofidence interval and individual tracks shaded. Dotted line shows a simple relay model could explain the kinetics observed.

the circuit to appear more like a simple relay system (as in Figure 3A).

Indeed, when compared with unperturbed waves, cells treated with the NADPH oxidase inhibitor diphenyleneiodonium chloride (DPI) produce a single swarming wave that does not self-extinguish and instead continues to propagate from the target out of the region of interest (ROI) (or until colliding with another propagating wave) (Figures 3E, 3F, and S3E; Video S3). Because DPI affects cell-autonomous roles of NADPH oxidase activity (like membrane depolarization) 55-57 as well as the

potential paracrine roles of released ROS, ^{58,59} we next investigated the role of extracellular reactive oxygen species (ROS) through the use of ROS scavengers catalase and superoxide dismutase. This extracellular ROS inhibition did not elicit a significant change in wave-stopping behaviors nor maximum wave size (Figure 3G). In contrast, DPI-drugged cells produce convex wave kinetics that are consistent with a simple relay model within the entire boundary of the largest ROI possible for both targets spaced 1 and 1.5 mm apart (Figures 3H and S3D–S3G). These results suggest a cell-autonomous role of NADPH oxidase



activation in LTB4 production, consistent with previous reports. ⁴⁷ To ensure that this effect on wave dynamics is not an off-target of DPI, we analyzed neutrophils from chronic granulomatosis disease (CGD) patients who have a genetic defect in neutrophil NADPH oxidase machinery. ⁵³ Similar to DPI-treated healthy donor cells, CGD neutrophils also exhibit non-extinguishing wave dynamics within our largest possible ROI (Figure S3B). Although both DPI-inhibited cells and CGD cells elicited strong recruitment within a signaling event, they only generate a single large wave compared with the multiple waves observed in unperturbed, healthy cells (Figure S3C; Video S3).

Modeling a self-extinguishing relay based on a positive feedback active relay coupled with an activation-dependent non-diffusible inhibitor

We next sought to mathematically model potential circuit architectures that could account for the observed self-extinguishing neutrophil swarming waves. The first architecture we explored involved a diffusive co-permissive cue released at the core. This model was quickly discarded due to its dependence on a biologically implausible diffusion coefficient and its inability to explain the lack of wave termination following NADPH oxidase inhibition (see Methods S1; Figures S4H–S4J).

Turning our attention to potential inhibitory circuits that could underlie a self-extinguishing relay, we found one prior example of a self-extinguishing relay model attempting to explain the spatial regulation of blood clotting. In this work, a one-dimensional (1D) model of two separately relayed, *diffusive activator* and *diffusive inhibitor* cues generated a fixed radius of relayed activation in a cell-free system. We explored whether this model could create wave-stopping solutions in two-dimensional (2D) and three-dimensional (3D) diffusive environments and were unable to find stable solutions for the diffusive conditions in our assay (Methods S1). Furthermore, this class of models requires a diffusible inhibitor and is, therefore, incompatible with the cell-autonomous role that NADPH oxidase activation plays in LTB₄ production (Figure 3G). 47

To address these deficiencies in both model classes explored, we constructed a mathematical model based on a diffusive activator cue and a non-diffusive local inhibitor that is consistent with our understanding of neutrophil self-extinguishing relay waves. Our model relies on a single diffusive ligand that triggers different cellular responses at two different threshold concentrations of the ligand (Figure 4A). This idea is inspired by previous work showing that LTB4 can evoke different cellular responses at different ligand thresholds. 61-65 In particular, BLT1 has been shown to exhibit a "stepwise" phosphorylation pattern that allows the receptor to selectively trigger different arms of the Gprotein-coupled receptor signaling cascade at low (10 nM) and high (100 nM) amounts of LTB4.64,65 In our self-extinguishing relay model, cells exposed to a low threshold of activating ligand (L₁) initiate a non-diffusive, local inhibition circuit that starts to limit the potential of that cell to create more activating ligand. This low threshold for negative feedback is consistent with previous reports of sub-nanomolar amounts of LTB4 inhibiting further LTB₄ production in human neutrophils.⁴⁹ When the cell is exposed to a higher threshold of activating ligand (L_0) , it begins to create more activating ligand locally if the local inhibition has not yet exceeded some amount (I). This local creation of ligand

serves to help trigger neighboring cells to further relay the activating cue and is the basis for positive feedback in the system. This higher threshold for positive feedback is consistent with higher doses of LTB4, shown to activate and augment key steps in LTB4 synthesis/release. Our current model is likely an oversimplification of the true positive feedback present, which likely involves a feedforward cascade in which LTB4 generates and mobilizes arachidonic acid, which then acts in conjunction with LTB4 to further LTB4 synthesis. 40,42,43

For our self-extinguishing relay model, we can expand on the analysis for traveling wave solutions first explored in previous work³⁸ to find four distinct phases for waves that have self-extinguishing relay behaviors. In Figure 4B, the initiation of a wave event begins with the low threshold for inhibitor circuit initiation (spatially drawn as r₁) spaced closely to the higher threshold for activator production (spatially drawn as r₀). As a result, for cells close to the target, only a small amount of inhibition is generated before such cells cross the threshold for activator production and effective activator cue relay occurs. For each relaying cell that has crossed both the r₁ and r₀ threshold of activator, the intracellular inhibition continues until an inhibitory maximum threshold value (I) is reached, stopping the production of further activating cue. This shutoff effect creates a time-delayed zone of cells that are no longer able to relay (spatially drawn as r₂). Because the inhibition circuit limits relay behind the propagation front, cells participating in the relay do so in a pulsatile manner. At increasing distances away from the target, the relay threshold is passed closer in time to the cellular shutoff event, limiting the window for activator production until the effective "pulse duration" falls below a critical value, thereby terminating active relay at the wavefront (Figure S4B).

Consistent with our experimental observations, both continuous and discrete agent-based models generate fields of diffusive activating cue that propagate via a relay that has self-terminating properties (Figures 4C and S4F; Video S4). Our model also shows a good agreement with experimentally observed relay propagation kinetics, stopping behavior, and final maximum radius values (Figure 4D). By turning off inhibition in our model, we can recover simple relay propagation solutions like those observed in DPI-treated cells and CGD patient cells (Figure S4G; Video S4). In our formal analytical treatment of the continuous model, we identify key mathematical conditions that are necessary to generate self-extinguishing solutions and demonstrate the stability of the modeling parameters (Methods S1; Figures S4C–S4E).

Neutrophils tune the size and number of swarming waves in response to differences in initial cell density

To investigate the physiological significance of multiple self-extinguishing waves, we next sought to probe the relation between wave size/number and the resulting cell movement and recruitment toward a target. We hypothesized that these wave parameters may be actively adjusted to enable robust homeostatic control of neutrophil recruitment across a wide range of initial conditions. First, we analyzed cell movement following a single, well-separated wave event. Single-cell tracks were aligned based on the time at which they entered the wave to determine the average radial migration velocity profile (Figure 5A; unaligned track averages: Figure S5A). Upon entering a wave, neutrophils





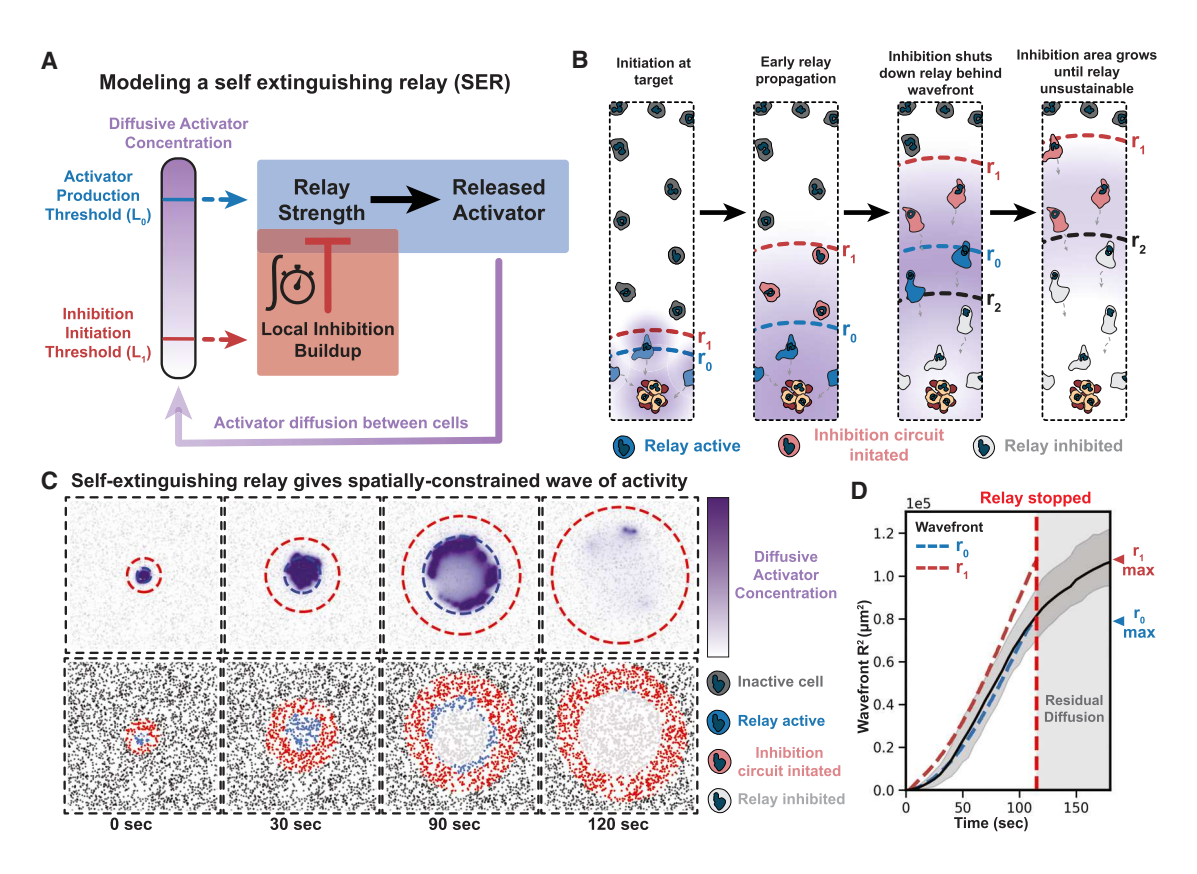


Figure 4. Modeling a self-extinguishing relay based on a positive feedback active relay coupled with an activation-dependent non-diffusible inhibitor

(A) In this model, a single diffusive ligand propagates through a field of cells. At a low threshold of this extracellular ligand, cells initiate a non-diffusive local inhibition circuit that limits the relay potential of a given cell; once this inhibition accumulates to a critical level, cells lose their ability to participate in relay. At a higher threshold of the extracellular ligand, cells begin to emit more of the activating ligand unless the inhibition has accumulated to a sufficient level to block this process.

(B) Based on the dynamics of ligand (purple) diffusion, the wavefront corresponding to the low inhibitory threshold (r_1) , dotted red line) moves more rapidly than the wavefront corresponding to the high activating threshold (r_0) , dotted blue line). Because of the difference in propagation speeds between the two thresholds, cells further from the target have longer periods of inhibition buildup (red cells) before initiating positive feedback (blue cells), dampening the relay strength as it moves away from an initiation site until the relay eventually terminates. As the inhibitory circuit reaches a shutoff threshold value (I), a zone of deactivated cells (indicated by r_2 , light gray cells) grows behind the wavefront, ultimately overtaking and destabilizing further wave propagation. Non-activated cells are in dark gray.

(C) Discrete simulations of this model yield a wave of propagating extracellular ligand that moves by active relay close to the initiation site before attenuating and eventually terminating. Diffusive activator gradient (purple) plotted with r_0 (blue) and r_1 (red) overlaid (top). Cell state plotted for same simulation as top panels to demonstrate how activated cells evolve from relaying to shutting off and terminating further relay propagation (bottom).

(D) Because our cellular readout is calcium and not receptor activation, we predict that a calcium pulse occurs between the low (L_1) and high (L_0) thresholds of our model. Our model generates simulations that match both early-wave relay kinetics and predict the final wave radius as being within the r_1 lower threshold boundary, after relay shutoff residual diffusion dominates late wave propagation. Experimental data taken from a subset of similarly sized waves with similar propagation kinetics averaged over time with 95% confidence. Wave n = 5. volunteer N = 2.

execute a discrete "run" of movement toward the wave center and then revert to random, slower movement, similar to the responses of *Dictyostelium* to waves of cyclic AMP (cAMP) during aggregation. 11,66 Such a "step" of movement inwards is consistent with the expected behavior from our self-extinguishing model where the chemotactic gradient decays behind the wavefront as the relay becomes dominated by the local inhibitory mechanism. These data indicate that a single wave event does not recruit all cells to the center in one burst. To expand our analysis to multiple waves, we integrated the radial movement of all cells within a wave event around a single target (Figures 5B and S5B). Each wave elicited the recruitment of a group of neutrophils toward a given target, with larger wave events more potently recruiting cells compared with smaller wave events (Video S5). When analyzed across many experiments and donors, the total integrated wave

area correlated strongly with the integrated radial movement of the cells within wave events (Figure 5C).

To investigate how swarming responses depend on starting conditions, we next varied the initial cell seeding density in our assay. At lower cell densities, there is an increase in the integrated calcium signaling area across all waves emanating from a single target (Figure 5D). As seeding density increases, neutrophils attenuate swarming responses by limiting both the size and number of waves emitted from a given target (Figures 5E and 5F; Video S5).

Healthy neutrophils can self-limit recruitment unlike CGD patient neutrophils

We next investigated whether the tuning of wave size and number enables consistent levels of neutrophil accumulation



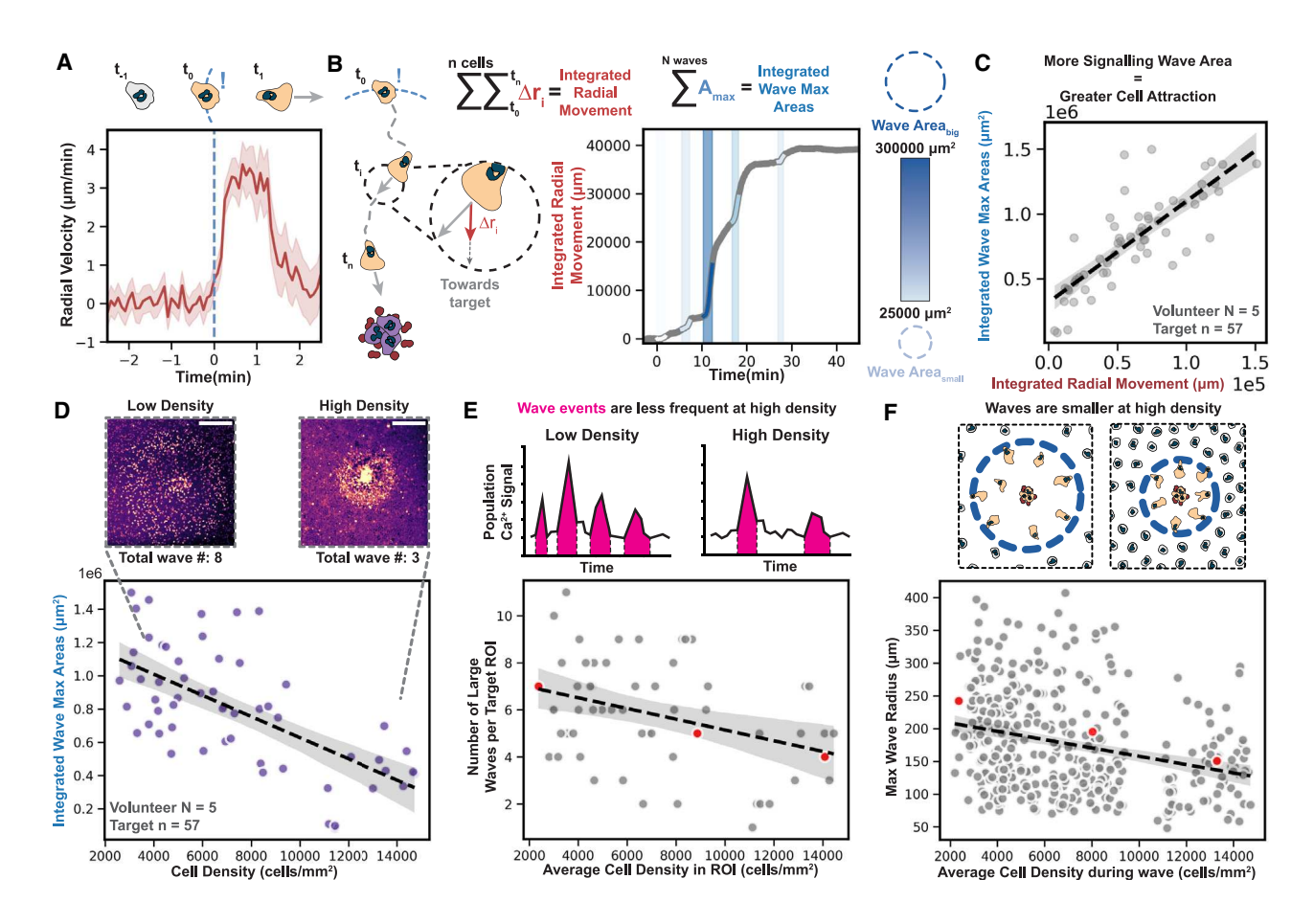


Figure 5. Neutrophils tune the size and number of swarming waves in response to differences in initial cell density

(A) Averaged radial velocities of neutrophil movement toward a target following time of exposure to swarming wave with 95% confidence interval plotted for 1,758 cell tracks. A single wave produces a transient bolus of neutrophil recruitment.

(B) All cellular tracks inside a wave are integrated for their radial movement (cell track n = 5,813); multiple wave events for the same target are plotted as shaded areas colored by maximum final area for an example ROI. Each wave induces a bolus of neutrophil movement toward the target, with larger waves inducing larger neutrophil responses.

(C) Integrated radial movement of all cell tracks and integrated wave maximum area measurements, calculated across 57 target ROIs, demonstrate the strong positive correlation between wave signaling area and movement toward a target. Linear fit slope: $7.8 \mu m \pm 0.8$, 95% confidence interval. A control where all cell tracks are considered is in Figure S5C.

(D) Relation of seeding density to cell accumulation at target. Integrated wave maximum area measurements taken for each target ROI over 45 min. Linear fit slope: $-6.3 \times 10^4 \ \mu\text{m}^2$ per 1,000 cells/mm² $\pm 1 \times 10^4$, 95% confidence interval. Lower cell densities elicit larger and more numerous swarming waves; representative panel insets scale bars, 200 μ m.

(E) The number of waves emanating from a given target are inversely correlated with the seeding density of cells surrounding the target. Linear fit slope: -0.2 waves per 1,000 cells/mm² \pm 0.07, 95% confidence interval. Red dots refer to representative Ca²⁺ traces in Figure S5D.

(F) The maximum radius of waves emanating from a given target are also inversely correlated with the seeding density of cells surrounding a target. Linear fit slope: -6.4 mm per 1,000 cells/mm² ± 1.0, 95% confidence. Red dots refer to representative wave events in Figure S5E.

across a range of initial cell densities. For this purpose, we assayed the kinetics of neutrophil accumulation and swarming wave responses for a range of starting cell densities (Figure 6A). At low seeding densities, we observed multiple large waves underlying swarming and accumulation of cells at the target. At higher seeding density, we observed similar accumulation at the target, but this is achieved by fewer and smaller waves (Figure 6B). This near-constant recruitment over a range of starting densities suggests homeostasis in the swarming response. To extend this observation, we quantified neutrophil recruitment to similarly sized sites of heat-killed *Candida albicans* over a 6-fold range of seeding densities

after 60 min (Figure S6B). Across this range of starting conditions, there was a near-constant accumulation of neutrophils at the target, with targets at the lowest densities attracting approximately 85% of the cells attracted at the highest cell densities (compared with 6-fold differences that would be expected for a non-homeostatic proportional system) (Figures 6C, 6D, and S6C). Because CGD patient neutrophils are defective in the negative feedback circuit that is needed to constrain wave size, we predicted that these cells should exhibit a defective homeostat and therefore recruit cells more proportional to their starting density; this is indeed the case (Figures 6E, 6F, S6D, and S6E).

Article



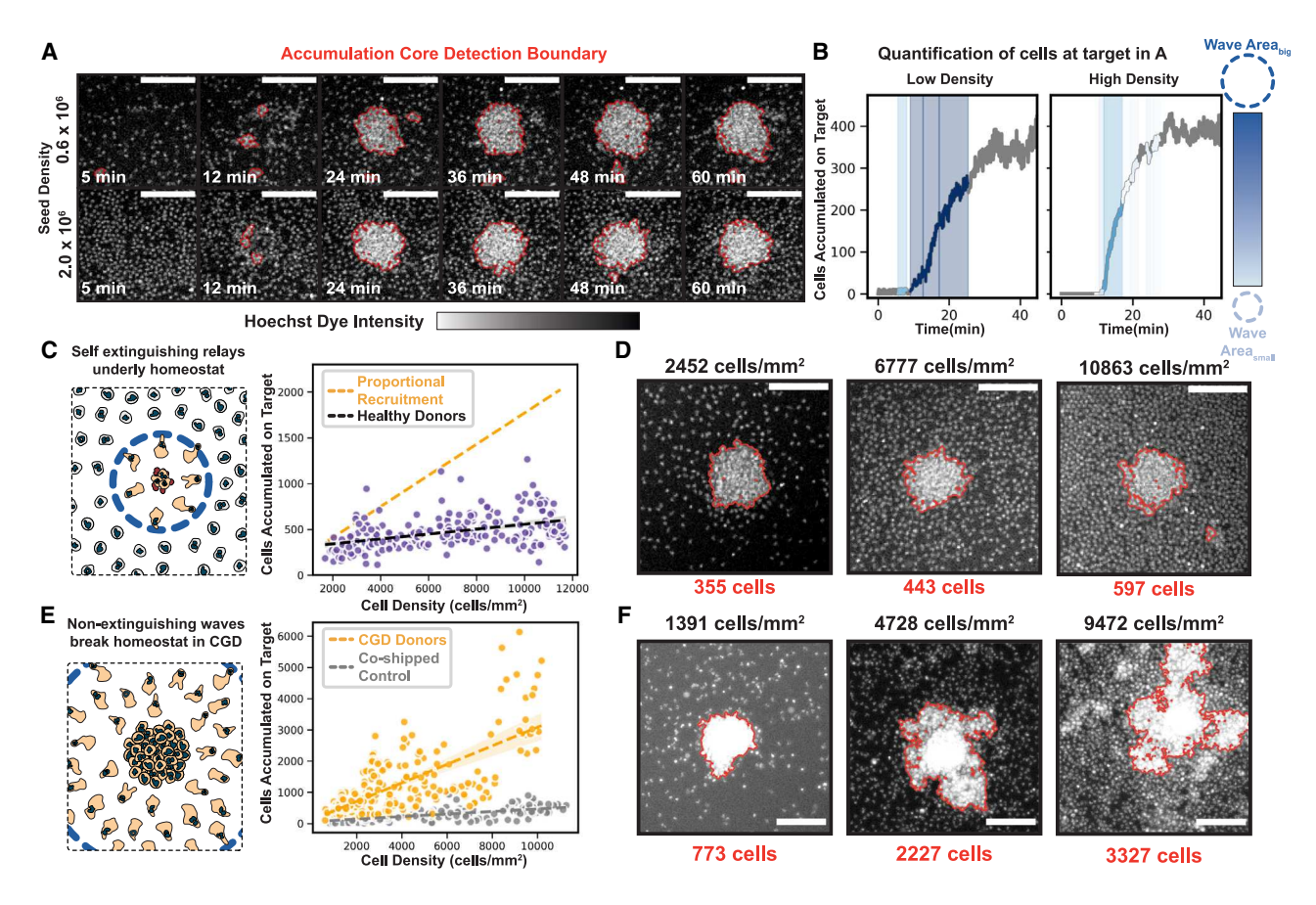


Figure 6. Healthy neutrophils can self-limit recruitment unlike CGD patient neutrophils

(A) We used Hoechst nuclear staining to assay the dynamics of neutrophil accumulation at the fungal target over a range of starting cell densities; scale bars, $100 \mu m$.

(B) Signaling waves for each target in (A) are plotted as shaded areas colored by maximum final area as in Figure 5B. Each wave contributes to neutrophil accumulation at the target. Both high and low seeding densities result in the same final cell accumulation at the target, and this is accomplished by larger and more frequent waves for cells at lower seeding densities.

(C) Z stack measurements taken across multiple ROIs per well 60 min after seeding swarming assays at different cell densities. Accumulation measured as integrated fluorescence at target site divided by median single-cell nuclear fluorescence. Only a small change in final neutrophil target accumulation is seen over a 6-fold range of cell swarming densities, compared with expectation for swarming directly proportional to cell density (proportional recruitment, orange line). Linear fit slope: 27 cells accumulate at target site per 1,000 cells/mm² ± 4 cells; 95% confidence interval.

(D) Representative grayscale images given of Hoechst intensity for in-focus z plane of an ROI with the accumulation boundary indicated. Scale bars, $100 \mu m$. (E) Widefield measurements taken across multiple ROIs per well 60 min after seeding swarming assays with different cell densities of either control donor cells or CGD (NADPH-oxidase-defective) human donor cells. Accumulation measured similar to (D), see STAR Methods. CGD linear fit line slope: 297 cells accumulate at a target per $1,000 \text{ cells/mm}^2 \pm 19 \text{ cells}$, 95% confidence interval (volunteer N = 4, target n = 253). Healthy control linear fit line slope: 40 cells accumulate at a target per $1,000 \text{ cells/mm}^2 \pm 4 \text{ cells}$ (volunteer N = 3, target n = 157).

(F) Representative accumulations of CGD cells are shown with their corresponding seeding cell densities. Scale bars, 100 µm.

DISCUSSION

By applying quantitative methods to a key dynamic readout of cell-cell signaling in a highly controllable *ex vivo* swarming assay, our work reveals self-extinguishing chemoattractant waves that control human neutrophil recruitment to sites of heat-killed *Candida albicans*. These waves propagate through an LTB₄-dependent active relay (Figure 2), and the self-extinguishing of these waves depends on a NADPH-oxidase-based negative feedback loop (Figures 3 and 4). The self-extinguishing property of these waves enables neutrophils to leverage positive feedback amplification without a runaway reaction that would otherwise result in unconstrained recruitment (Fig-

ures 5 and 6). Furthermore, the propagated waves generate temporally evolving, spatially sharp guidance cues that have been shown to enable more effective chemotaxis than static spatial gradients. ⁶⁶⁻⁶⁹ Behind a wavefront, decaying gradients could further prevent cells from over accumulating at the core of swarms as cellular memory mechanisms lose strength and as chemotaxis-inhibitory LTB4 metabolites accumulate. ^{68,70,71} Self-organizing chemoattractant gradients are seen in a wide diversity of other multicellular settings—from Dictyostelium chemotaxis and aggregation, ^{9-12,68,72} to cancer cell dispersal, ⁶ to embryonic morphogenesis ^{7,73,74}—and have a number of considerable advantages relative to fixed-source and sink gradients. ^{69,75,76}



Based on our work, there are interesting parallels between neutrophil recruitment during swarming and Dictyostelium recruitment during aggregation. Both systems use active relay mechanisms to generate the self-organizing gradients of chemoattractants that regulate collective migration. Both systems need to limit the number of cells recruited to a given recruitment site. Although controlled recruitment is critical for the proper regulation of multicellular morphogenesis in *Dictyostelium*, neutrophils require controlled recruitment to balance collateral tissue damage and optimal host defense. Importantly, Dictyostelium aggregation waves are not inherently self-limiting but instead rely on the interference of multiple aggregation sites to enable a large field of responsive Dictyostelium to be partitioned into multiple appropriately sized aggregation centers. In contrast, neutrophils require flexibility in responding to single or multiple simultaneous aggregation sites and thus deploy a fundamentally different selfextinguishing relay to enable recruitment sites to individually self-limit, whether there is one site or many.

Our work reveals surprising robustness in the swarming process in which a near-constant number of cells are recruited over a significant range of initial cell concentrations. The self-extinguishing nature of the relay enables the system to adjust the number and size of swarming waves for this homeostatic control of neutrophil recruitment. Disruption of this homeostat has severe consequences for inflammation *in vivo*. CGD patient neutrophils (that are defective in NADPH oxidase activation) are known to overproduce LTB₄ and hyperaccumulate at sites of injury/infection *in vitro* and *in vivo*. ^{31,47,52,54,77,78} Our work shows that these cells are defective in a key negative feedback arm that limits the spatial range of swarming signals and therefore lack one of the homeostats that normally constrains cell swarming.

Beyond our ex vivo system, it will be interesting to probe how other cell types influence the initiation, kinetics, and termination of neutrophil swarm waves. 20-22,79 We have focused on heatkilled Candida albicans-triggered neutrophil swarming (whose closest parallel is likely an infected lymph node), 21,26 but it will be interesting to compare how sterile injury 19,21,28,80 and combined injury/infection 19,26 change the dynamics of the swarming process. Although other swarming terminators (such as Grk2 activation)¹⁷ control the duration of swarming, the NADPH oxidase negative feedback circuit studied in our work also controls the spatial range of neutrophil swarming. It will be interesting to probe how these swarming termination programs relate to one another. Finally, as there are a number of other human diseases with known swarming defects, 81-83 it will be interesting to determine how these disease states interact with our model parameters and affect the self-extinguishing relay system we study in this work.

Limitations of the study

Our work captures several key features of neutrophil swarming, including LTB₄-based active relay and NADPH-oxidase-dependent wave termination. However, there are some experimental features that our self-extinguishing relay model does not capture yet. For example, we do not yet understand the inverse relation between cell density and wave size that is likely critical for constant neutrophil recruitment over a range of starting conditions. This behavior presumably necessitates additional diffusible inhibitors, like adenosine, 43,48,84 that can be shared between cells

and act as global quorum sensors. We also do not explicitly model the process of wave initiation. In contrast to the highly periodic initiation events seen in *Dictyostelium* cAMP aggregation waves, ¹² neutrophil swarming waves are less regular, and the basis of neutrophil swarming wave initiation is unknown. Finally, our *ex vivo* system likely over-simplifies signal propagation between neutrophils and it will be interesting to see how the system observed here translates into the *in vivo* context.

STAR*METHODS

Detailed methods are provided in the online version of this paper and include the following:

- KEY RESOURCES TABLE
- RESOURCE AVAILABILITY
 - Lead contact
 - Materials availability
 - Data and code availability
- EXPERIMENTAL MODEL AND STUDY PARTICIPANT DETAILS
- METHOD DETAILS
 - Neutrophil Isolation Protocol
 - o CGD Cell Isolation
 - Neutrophil Swarming Chip Protocol
 - Neutrophil Swarming Imaging Protocol
 - o CGD Donor Cell Accumulation Imaging
 - O CGD Donor Calcium Imaging
 - Simulation Methods
- QUANTIFICATION AND STATISTICAL ANALYSIS
 - o Image Quantification
 - o ARCOS Wave Tracking
 - Statistical Analysis

SUPPLEMENTAL INFORMATION

Supplemental information can be found online at https://doi.org/10.1016/j. devcel.2024.06.003.

ACKNOWLEDGMENTS

We thank members of the Weiner, Amir, and Irimia lab for helpful discussions, particularly Nick Martin and Henry De Belly for a critical reading of the manuscript. We thank Paul Dieterle and Allyson Sgro for their detailed feedback and advice regarding the theoretical model. We thank Henry Showell for his insight and advice regarding LTB4 signaling and synthesis pathways. We also thank the blood donors and phlebotomists without whom this project would have been impossible. The micropatterned coverslips were manufactured at the BioMEMS Core at Massachusetts General Hospital, BIIL 315 was kindly provided by Boehringer Ingelheim via its open innovation platform opnMe, available at https://opnme.com. Finally, we would like to thank the Center for Advanced Light Microscopy-Nikon Imaging Center at UCSF for their support in using the CREST/C2 confocal microscope. This work was supported by the National Institutes of Health grants GM118167, Al176658, GM092804, and Al132638. O.D.W. is also supported by the National Science Foundation/Biotechnology and Biological Sciences Research Council grant 2019598, the National Science Foundation Center for Cellular Construction grant DBI-1548297, and the Novo Nordisk Foundation grant for the Center for Geometrically Engineered Cellular Systems NNF17OC0028176. E.S. was further supported by the AHA predoctoral fellowship. M.K.M. also receives support from the Department of Defense grant HU00012020011. A.A. was supported by the Clore Center for Biological Physics and the NSF CAREER grant 1752024. D.I. is further supported by the Shriners Hospitals for Children 71010-BOS-22. C.Z. received support for this work from the Intramural Research Program of the National Institutes of Health Clinical Center and the National Institute of Allergy and Infectious Diseases.

Article



AUTHOR CONTRIBUTIONS

Conceptualization: E.S. and O.D.W.; methodology: E.S. and O.D.W.; investigation: E.S., J.S.K., and O.D.W.; software: E.S. and D.P.; formal analysis (math modeling): D.P., W.J., and A.A.; resources: C.G., A.H., M.D., B.V., C.S.Z., and D.I.; visualization: E.S.; funding acquisition: O.D.W., A.A., D.I., and M.K.M.; project administration: E.S. and O.D.W.; supervision: O.D.W.; writing – original draft: E.S., O.D.W., and D.P.; writing – review & editing: E.S., O.D.W., D.P., A.A., W.J., D.I., and M.K.M.

DECLARATION OF INTERESTS

The authors declare no competing interests.

Received: November 22, 2023 Revised: March 16, 2024 Accepted: June 7, 2024 Published: July 5, 2024

REFERENCES

- Chandra, V., Gal, A., and Kronauer, D.J.C. (2021). Colony expansions underlie the evolution of army ant mass raiding. Proc. Natl. Acad. Sci. USA 118, e2026534118. https://doi.org/10.1073/pnas.2026534118.
- Gordon, D.M. (2019). The Ecology of Collective Behavior in Ants. Annu. Rev. Entomol. 64, 35–50. https://doi.org/10.1146/annurev-ento-011118-111923
- Parrish, J.K., and Edelstein-Keshet, L. (1999). Complexity, pattern, and evolutionary trade-offs in animal aggregation. Science 284, 99–101. https://doi.org/10.1126/science.284.5411.99.
- LaChance, J., Suh, K., Clausen, J., and Cohen, D.J. (2022). Learning the rules of collective cell migration using deep attention networks. PLOS Comput. Biol. 18, e1009293. https://doi.org/10.1371/journal.pcbi. 1009293
- Sun, Y., Reid, B., Zhang, Y., Zhu, K., Ferreira, F., Estrada, A., Sun, Y., Draper, B.W., Yue, H., Copos, C., et al. (2023). Electric field-guided collective motility initiation of large epidermal cell groups. Mol. Biol. Cell 34, ar48. https://doi.org/10.1091/mbc.E22-09-0391.
- Muinonen-Martin, A.J., Susanto, O., Zhang, Q., Smethurst, E., Faller, W.J., Veltman, D.M., Kalna, G., Lindsay, C., Bennett, D.C., Sansom, O.J., et al. (2014). Melanoma cells break down LPA to establish local gradients that drive chemotactic dispersal. PLoS Biol. 12, e1001966. https://doi.org/ 10.1371/journal.pbio.1001966.
- Donà, E., Barry, J.D., Valentin, G., Quirin, C., Khmelinskii, A., Kunze, A., Durdu, S., Newton, L.R., Fernandez-Minan, A., Huber, W., et al. (2013). Directional tissue migration through a self-generated chemokine gradient. Nature 503, 285–289. https://doi.org/10.1038/nature12635.
- Gregor, T., Fujimoto, K., Masaki, N., and Sawai, S. (2010). The Onset of Collective Behavior in Social Amoebae. Science 328, 1021–1025. https://doi.org/10.1126/science.1183415.
- Tomchik, K.J., and Devreotes, P.N. (1981). Adenosine 3',5'-monophosphate waves in Dictyostelium discoideum: a demonstration by isotope dilutionfluorography. Science 212, 443–446. https://doi.org/10.1126/science. 6259734.
- Sawai, S., Thomason, P.A., and Cox, E.C. (2005). An autoregulatory circuit for long-range self-organization in Dictyostelium cell populations. Nature 433, 323–326. https://doi.org/10.1038/nature03228.
- Dormann, D., and Weijer, C.J. (2001). Propagating chemoattractant waves coordinate periodic cell movement in Dictyostelium slugs. Development 128, 4535–4543. https://doi.org/10.1242/dev.128.22.4535.
- Sgro, A.E., Schwab, D.J., Noorbakhsh, J., Mestler, T., Mehta, P., and Gregor, T. (2015). From intracellular signaling to population oscillations: bridging size- and time-scales in collective behavior. Mol. Syst. Biol. 11, 779. https://doi.org/10.15252/msb.20145352.
- Dowdell, A., Paschke, P.I., Thomason, P.A., Tweedy, L., and Insall, R.H. (2023). Competition between chemoattractants causes unexpected

- complexity and can explain negative chemotaxis. Curr. Biol. 33, 1704–1715.e3. https://doi.org/10.1016/j.cub.2023.03.006.
- Ley, K., Hoffman, H.M., Kubes, P., Cassatella, M.A., Zychlinsky, A., Hedrick, C.C., and Catz, S.D. (2018). Neutrophils: New insights and open questions. Sci. Immunol. 3, eaat4579. https://doi.org/10.1126/sciimmunol.aat4579.
- Kolaczkowska, E., and Kubes, P. (2013). Neutrophil recruitment and function in health and inflammation. Nat. Rev. Immunol. 13, 159–175. https://doi.org/10.1038/nri3399.
- Peiseler, M., and Kubes, P. (2019). More friend than foe: the emerging role of neutrophils in tissue repair. J. Clin. Invest. 129, 2629–2639. https://doi. org/10.1172/JCI124616.
- Kienle, K., Glaser, K.M., Eickhoff, S., Mihlan, M., Knöpper, K., Reátegui, E., Epple, M.W., Gunzer, M., Baumeister, R., Tarrant, T.K., et al. (2021). Neutrophils self-limit swarming to contain bacterial growth in vivo. Science 372, eabe7729. https://doi.org/10.1126/science.abe7729.
- Sun, D., and Shi, M. (2016). Neutrophil swarming toward Cryptococcus neoformans is mediated by complement and leukotriene B4. Biochem. Biophys. Res. Commun. 477, 945–951. https://doi.org/10.1016/j.bbrc. 2016.07.005
- Poplimont, H., Georgantzoglou, A., Boulch, M., Walker, H.A., Coombs, C., Papaleonidopoulou, F., and Sarris, M. (2020). Neutrophil Swarming in Damaged Tissue Is Orchestrated by Connexins and Cooperative Calcium Alarm Signals. Curr. Biol. 30, 2761–2776.e7. https://doi.org/10. 1016/j.cub.2020.05.030.
- Reátegui, E., Jalali, F., Khankhel, A.H., Wong, E., Cho, H., Lee, J., Serhan, C.N., Dalli, J., Elliott, H., and Irimia, D. (2017). Microscale arrays for the profiling of start and stop signals coordinating human-neutrophil swarming. Nat. Biomed. Eng. 1, 0094. https://doi.org/10.1038/s41551-017-0094.
- Lämmermann, T., Afonso, P.V., Angermann, B.R., Wang, J.M., Kastenmüller, W., Parent, C.A., and Germain, R.N. (2013). Neutrophil swarms require LTB4 and integrins at sites of cell death in vivo. Nature 498, 371–375. https://doi.org/10.1038/nature12175.
- Uderhardt, S., Martins, A.J., Tsang, J.S., Lämmermann, T., and Germain, R.N. (2019). Resident Macrophages Cloak Tissue Microlesions to Prevent Neutrophil-Driven Inflammatory Damage. Cell 177, 541–555.e17. https://doi.org/10.1016/j.cell.2019.02.028.
- Jiwa, K., Ward, C., Parry, G., Brodlie, M., Lordan, J., Fisher, A., and Garnett, J. (2020). Immunohistochemical evidence of increased neutrophil swarms in Cystic Fibrosis lung removed at transplantation. Eur. Respir. J. 56, 698. https://doi.org/10.1183/13993003.congress-2020.698.
- Mawhin, M.-A., Tilly, P., Zirka, G., Charles, A.-L., Slimani, F., Vonesch, J.-L., Michel, J.-B., Bäck, M., Norel, X., and Fabre, J.-E. (2018). Neutrophils recruited by leukotriene B4 induce features of plaque destabilization during endotoxaemia. Cardiovasc. Res. 114, 1656–1666. https://doi.org/10.1093/cvr/cvy130.
- Isles, H.M., Loynes, C.A., Alasmari, S., Kon, F.C., Henry, K.M., Kadochnikova, A., Hales, J., Muir, C.F., Keightley, M.-C., Kadirkamanathan, V., et al. (2021). Pioneer neutrophils release chromatin within in vivo swarms. eLife 10, e68755. https://doi.org/10.7554/ eLife.68755.
- Chtanova, T., Schaeffer, M., Han, S.-J., van Dooren, G.G., Nollmann, M., Herzmark, P., Chan, S.W., Satija, H., Camfield, K., Aaron, H., et al. (2008).
 Dynamics of neutrophil migration in lymph nodes during infection. Immunity 29, 487–496. https://doi.org/10.1016/j.immuni.2008.07.012.
- Khazen, R., Corre, B., Garcia, Z., Lemaître, F., Bachellier-Bassi, S., d'Enfert, C., and Bousso, P. (2022). Spatiotemporal dynamics of calcium signals during neutrophil cluster formation. Proc. Natl. Acad. Sci. USA 119, e2203855119. https://doi.org/10.1073/pnas.2203855119.
- Ng, L.G., Qin, J.S., Roediger, B., Wang, Y., Jain, R., Cavanagh, L.L., Smith, A.L., Jones, C.A., de Veer, M., Grimbaldeston, M.A., et al. (2011).
 Visualizing the Neutrophil Response to Sterile Tissue Injury in Mouse Dermis Reveals a Three-Phase Cascade of Events. J. Invest. Dermatol. 131, 2058–2068. https://doi.org/10.1038/jid.2011.179.



Developmental Cell

- 29. Nauseef, W.M. (2023). Human neutrophils ≠ murine neutrophils: Does it matter? Immunol. Rev. 314, 442-456. https://doi.org/10.1111/imr.13154.
- 30. Siwicki, M., and Kubes, P. (2023). Neutrophils in host defense, healing, and hypersensitivity: Dynamic cells within a dynamic host. J. Allergy Clin. Immunol. 151, 634-655. https://doi.org/10.1016/j.jaci.2022.12.004.
- 31. Hopke, A., Scherer, A., Kreuzburg, S., Abers, M.S., Zerbe, C.S., Dinauer, M.C., Mansour, M.K., and Irimia, D. (2020). Neutrophil swarming delays the growth of clusters of pathogenic fungi. Nat. Commun. 11, 2031. https://doi.org/10.1038/s41467-020-15834-4.
- 32. Molski, T.F., Naccache, P.H., Borgeat, P., and Sha'afi, R.I. (1981). Similarities in the mechanisms by which formyl-methionyl-leucyl-phenylalanine, arachidonic acid and leukotriene B4 increase calcium and sodium influxes in rabbit neutrophils. Biochem. Biophys. Res. Commun. 103, 227-232. https://doi.org/10.1016/0006-291x(81)91683-1.
- 33. Gagliardi, P.A., Grädel, B., Jacques, M.-A., Hinderling, L., Ender, P., Cohen, A.R., Kastberger, G., Pertz, O., and Dobrzyński, M. (2023). Automatic detection of spatio-temporal signaling patterns in cell collectives. J. Cell Biol. 222, e202207048. https://doi.org/10.1083/jcb.
- 34. Afonso, P.V., Janka-Junttila, M., Lee, Y.J., McCann, C.P., Oliver, C.M., Aamer, K.A., Losert, W., Cicerone, M.T., and Parent, C.A. (2012). LTB4 Is a Signal-Relay Molecule during Neutrophil Chemotaxis. Dev. Cell 22, 1079-1091. https://doi.org/10.1016/j.devcel.2012.02.003.
- 35. McDonald, P.P., McColl, S.R., Braquet, P., and Borgeat, P. (1994). Autocrine enhancement of leukotriene synthesis by endogenous leukotriene B4 and platelet-activating factor in human neutrophils. Br. J. Pharmacol. 111, 852-860. https://doi.org/10.1111/j.1476-5381.1994. tb14816 x
- 36. Fischer, J., Gresnigt, M.S., Werz, O., Hube, B., and Garscha, U. (2021). Candida albicans-induced leukotriene biosynthesis in neutrophils is restricted to the hyphal morphology. FASEB J. 35, e21820. https://doi. org/10.1096/fj.202100516RR.
- 37. Birke, F.W., Meade, C.J., Anderskewitz, R., Speck, G.A., and Jennewein, H.M. (2001). In vitro and in vivo pharmacological characterization of BIIL 284, a novel and potent leukotriene B(4) receptor antagonist. J. Pharmacol. Exp. Ther. 297, 458-466.
- 38. Dieterle, P.B., Min, J., Irimia, D., and Amir, A. (2020). Dynamics of diffusive cell signaling relays. eLife 9, e61771. https://doi.org/10.7554/eLife.61771.
- 39. McDonald, P.P., McColl, S.R., Naccache, P.H., and Borgeat, P. (1992). Activation of the human neutrophil 5-lipoxygenase by leukotriene B4. Br. J. Pharmacol. 107, 226-232. https://doi.org/10.1111/j.1476-5381.1992. tb14491.x.
- 40. Wijkander, J., O'Flaherty, J.T., Nixon, A.B., and Wykle, R.L. (1995). 5-lipoxygenase products modulate the activity of the 85-kDa phospholipase A2 in human neutrophils. J. Biol. Chem. 270, 26543-26549. https://doi. org/10.1074/jbc.270.44.26543.
- 41. Gilbert, N.C., Gerstmeier, J., Schexnaydre, E.E., Börner, F., Garscha, U., Neau, D.B., Werz, O., and Newcomer, M.E. (2020). Structural and mechanistic insights into 5-lipoxygenase inhibition by natural products. Nat. Chem. Biol. 16, 783-790. https://doi.org/10.1038/s41589-020-0544-7.
- 42. Burke, J.R., Davern, L.B., Gregor, K.R., and Tramposch, K.M. (1997). Leukotriene B4 stimulates the release of arachidonate in human neutrophils via the action of cytosolic phospholipase A2. Biochim. Biophys. Acta 1359, 80-88. https://doi.org/10.1016/s0167-4889(97)00094-3.
- 43. Surette, M.E., Krump, E., Picard, S., and Borgeat, P. (1999). Activation of leukotriene synthesis in human neutrophils by exogenous arachidonic acid: inhibition by adenosine A(2a) receptor agonists and crucial role of autocrine activation by leukotriene B(4). Mol. Pharmacol. 56, 1055-1062. https://doi.org/10.1124/mol.56.5.1055.
- 44. Shaffer, B.M. (1975). Secretion of cyclic AMP induced by cyclic AMP in the cellular slime mould Dictyostelium discoideum. Nature 255, 549-552. https://doi.org/10.1038/255549a0.
- 45. van Oss, C., Panfilov, A.V., Hogeweg, P., Siegert, F., and Weijer, C.J. (1996). Spatial pattern formation during aggregation of the slime mould

- Dictyostelium discoideum. J. Theor. Biol. 181, 203-213. https://doi.org/ 10.1006/itbi.1996.0126
- 46. Gelens, L., Anderson, G.A., and Ferrell, J.E., Jr. (2014). Spatial trigger waves: positive feedback gets you a long way. Mol. Biol. Cell 25, 3486-3493. https://doi.org/10.1091/mbc.E14-08-1306.
- 47. Song, Z., Huang, G., Chiquetto Paracatu, L., Grimes, D., Gu, J., Luke, C.J., Clemens, R.A., and Dinauer, M.C. (2020). NADPH oxidase controls pulmonary neutrophil infiltration in the response to fungal cell walls by limiting LTB4. Blood 135, 891-903. https://doi.org/10.1182/blood.2019003525.
- 48. Krump, E., Picard, S., Mancini, J., and Borgeat, P. (1997). Suppression of leukotriene B4 biosynthesis by endogenous adenosine in ligand-activated human neutrophils. J. Exp. Med. 186, 1401-1406. https://doi.org/10.1084/ iem.186.8.1401.
- 49. Fiedler, J., Wheelan, P., Henson, P.M., and Murphy, R.C. (1998). Exogenous Leukotriene B4 (LTB4) Inhibits Human Neutrophil Generation of LTB4 from Endogenous Arachidonic Acid During Opsonized Zymosan Phagocytosis. J. Pharmacol. Exp. Ther. 287, 150-156.
- 50. Yang, F., Suo, M., Weli, H., Wong, M., Junidi, A., Cummings, C., Johnson, R., Mallory, K., Liu, A.Y., Greenberg, Z.J., et al. (2023). Staphylococcus aureus α -toxin impairs early neutrophil localization via electrogenic disruption of store-operated calcium entry. Cell Rep. 42, 113394. https://doi.org/ 10.1016/j.celrep.2023.113394.
- 51. Serezani, C.H.C., Aronoff, D.M., Jancar, S., and Peters-Golden, M. (2005). Leukotriene B4 mediates p47phox phosphorylation and membrane translocation in polyunsaturated fatty acid-stimulated neutrophils. J. Leukoc. Biol. 78, 976–984. https://doi.org/10.1189/jlb.1004587.
- 52. Henrickson, S.E., Jongco, A.M., Thomsen, K.F., Garabedian, E.K., and Thomsen, I.P. (2018). Noninfectious Manifestations and Complications of Chronic Granulomatous Disease. J. Pediatric Infect. Dis. Soc. 7, S18-S24. https://doi.org/10.1093/jpids/piy014.
- 53. Roxo-Junior, P., and Simão, H.M.L. (2014). Chronic granulomatous disease: why an inflammatory disease? Braz. J. Med. Biol. Res. 47, 924-928. https://doi.org/10.1590/1414-431X20143735.
- 54. Hamasaki, T., Sakano, T., Kobayashi, M., Sakura, N., Ueda, K., and Usui, T. (1989). Leukotriene B4 metabolism in neutrophils of patients with chronic granulomatous disease: phorbol myristate acetate decreases endogenous leukotriene B4 via NADPH oxidase-dependent mechanism. Eur. J. Clin. Invest. 19, 404-411. https://doi.org/10.1111/j.1365-2362. 1989.tb00249.x.
- 55. Ahlin, A., Gyllenhammar, H., Ringertz, B., and Palmblad, J. (1995). Neutrophil membrane potential changes and homotypic aggregation kinetics are pH-dependent: studies of chronic granulomatous disease. J. Lab. Clin. Med. 125, 392-401.
- 56. Tintinger, G.R., Theron, A.J., Steel, H.C., and Anderson, R. (2001). Accelerated calcium influx and hyperactivation of neutrophils in chronic granulomatous disease. Clin. Exp. Immunol. 123, 254-263. https://doi. org/10.1046/j.1365-2249.2001.01447.x.
- 57. Henderson, L.M., Chappell, J.B., and Jones, O.T. (1987). The superoxidegenerating NADPH oxidase of human neutrophils is electrogenic and associated with an H+ channel. Biochem. J. 246, 325-329. https://doi. org/10.1042/bj2460325.
- 58. Katikaneni, A., Jelcic, M., Gerlach, G.F., Ma, Y., Overholtzer, M., and Niethammer, P. (2020). Lipid peroxidation regulates long-range wound detection through 5-lipoxygenase in zebrafish. Nat. Cell Biol. 22, 1049-1055. https://doi.org/10.1038/s41556-020-0564-2.
- 59. Yoo, S.K., Starnes, T.W., Deng, Q., and Huttenlocher, A. (2011). Lyn is a redox sensor that mediates leukocyte wound attraction in vivo. Nature 480, 109-112, https://doi.org/10.1038/nature10632.
- 60. Ataullakhanov, F.I., Guria, G.T., Sarbash, V.I., and Volkova, R.I. (1998). Spatiotemporal dynamics of clotting and pattern formation in human blood. Biochim. Biophys. Acta 1425, 453-468. https://doi.org/10.1016/ s0304-4165(98)00102-0.
- 61. Lundgren, S.M., Rocha-Gregg, B.L., Akdoğan, E., Mysore, M.N., Hayes, S., and Collins, S.R. (2023). Signaling dynamics distinguish high- and

Article



- low-priority neutrophil chemoattractant receptors. Sci. Signal. *16*, eadd1845. https://doi.org/10.1126/scisignal.add1845.
- Perkins, R.S., Lindsay, M.A., Barnes, P.J., and Giembycz, M.A. (1995). Early signalling events implicated in leukotriene B4-induced activation of the NADPH oxidase in eosinophils: role of Ca2+, protein kinase C and phospholipases C and D. Biochem. J. 310, 795–806. https://doi.org/10. 1042/bj3100795.
- Zinn, S., Sisignano, M., Kern, K., Pierre, S., Tunaru, S., Jordan, H., Suo, J., Treutlein, E.-M., Angioni, C., Ferreiros, N., et al. (2017). The leukotriene B4 receptors BLT1 and BLT2 form an antagonistic sensitizing system in peripheral sensory neurons. J. Biol. Chem. 292, 6123–6134. https://doi. org/10.1074/jbc.M116.769125.
- 64. Tatsumi, R., Aihara, S., Matsune, S., Aoki, J., Inoue, A., Shimizu, T., and Nakamura, M. (2023). Stepwise phosphorylation of BLT1 defines complex assemblies with β-arrestin serving distinct functions. FASEB J. 37, e23213. https://doi.org/10.1096/fj.202301440R.
- 65. Nakanishi, Y., Tan, M., Ichiki, T., Inoue, A., Yoshihara, J.-I., Maekawa, N., Takenoshita, I., Yanagida, K., Yamahira, S., Yamaguchi, S., et al. (2018). Stepwise phosphorylation of leukotriene B₄ receptor 1 defines cellular responses to leukotriene B₄. Sci. Signal. 11, eaao5390. https://doi.org/10.1126/scisignal.aao5390.
- Skoge, M., Yue, H., Erickstad, M., Bae, A., Levine, H., Groisman, A., Loomis, W.F., and Rappel, W.-J. (2014). Cellular memory in eukaryotic chemotaxis. Proc. Natl. Acad. Sci. USA 111, 14448–14453. https://doi. org/10.1073/pnas.1412197111.
- Geiger, J., Wessels, D., and Soll, D.R. (2003). Human polymorphonuclear leukocytes respond to waves of chemoattractant, like Dictyostelium. Cell Motil. Cytoskeleton 56, 27–44. https://doi.org/10.1002/cm.10133.
- Tweedy, L., Knecht, D.A., Mackay, G.M., and Insall, R.H. (2016). Self-Generated Chemoattractant Gradients: Attractant Depletion Extends the Range and Robustness of Chemotaxis. PLoS Biol. 14, e1002404. https://doi.org/10.1371/journal.pbio.1002404.
- Aranyosi, A.J., Wong, E.A., and Irimia, D. (2015). A neutrophil treadmill to decouple spatial and temporal signals during chemotaxis. Lab Chip 15, 549–556. https://doi.org/10.1039/c4lc00970c.
- Archambault, A.-S., Poirier, S., Lefebvre, J.-S., Robichaud, P.-P., Larose, M.-C., Turcotte, C., Martin, C., Provost, V., Boudreau, L.H., McDonald, P.P., et al. (2019). 20-Hydroxy- and 20-carboxy-leukotriene (LT) B4 downregulate LTB4-mediated responses of human neutrophils and eosinophils. J. Leukoc. Biol. 105, 1131–1142. https://doi.org/10.1002/JLB.MA0718-306R.
- Pettipher, E.R., Salter, E.D., Breslow, R., Raycroft, L., and Showell, H.J. (1993). Specific inhibition of leukotriene B4 (LTB4)-induced neutrophil emigration by 20-hydroxy LTB4: implications for the regulation of inflammatory responses. Br. J. Pharmacol. 110, 423–427. https://doi.org/10.1111/j.1476-5381.1993.tb13827.x.
- Noorbakhsh, J., Schwab, D.J., Sgro, A.E., Gregor, T., and Mehta, P. (2015). Modeling oscillations and spiral waves in Dictyostelium populations. Phys. Rev. E Stat. Nonlin. Soft Matter Phys. 91, 062711. https://doi.org/10.1103/PhysRevE.91.062711.
- 73. Boldajipour, B., Mahabaleshwar, H., Kardash, E., Reichman-Fried, M., Blaser, H., Minina, S., Wilson, D., Xu, Q., and Raz, E. (2008). Control of che-

- mokine-guided cell migration by ligand sequestration. Cell *132*, 463–473. https://doi.org/10.1016/j.cell.2007.12.034.
- Venkiteswaran, G., Lewellis, S.W., Wang, J., Reynolds, E., Nicholson, C., and Knaut, H. (2013). Generation and dynamics of an endogenous, selfgenerated signaling gradient across a migrating tissue. Cell 155, 674–687. https://doi.org/10.1016/j.cell.2013.09.046.
- Tweedy, L., Thomason, P.A., Paschke, P.I., Martin, K., Machesky, L.M., Zagnoni, M., and Insall, R.H. (2020). Seeing around corners: Cells solve mazes and respond at a distance using attractant breakdown. Science 369, eaay9792. https://doi.org/10.1126/science.aay9792.
- Insall, R.H. (2023). Receptors, enzymes and self-attraction as autocrine generators and amplifiers of chemotaxis and cell steering. Curr. Opin. Cell Biol. 81, 102169. https://doi.org/10.1016/j.ceb.2023.102169.
- Dinauer, M.C. (2019). Inflammatory consequences of inherited disorders affecting neutrophil function. Blood 133, 2130–2139. https://doi.org/10. 1182/blood-2018-11-844563.
- Song, Z., Bhattacharya, S., Clemens, R.A., and Dinauer, M.C. (2023).
 Molecular regulation of neutrophil swarming in health and disease:
 Lessons from the phagocyte oxidase. iScience 26, 108034. https://doi.org/10.1016/j.isci.2023.108034.
- Walters, N., Zhang, J., Rima, X.Y., Nguyen, L.T.H., Germain, R.N., Lämmermann, T., and Reátegui, E. (2021). Analyzing Inter-Leukocyte Communication and Migration In Vitro: Neutrophils Play an Essential Role in Monocyte Activation During Swarming. Front. Immunol. 12, 671546. https://doi.org/10.3389/fimmu.2021.671546.
- Park, S.A., Choe, Y.H., Park, E., and Hyun, Y.-M. (2018). Real-time dynamics of neutrophil clustering in response to phototoxicity-induced cell death and tissue damage in mouse ear dermis. Cell Adh. Migr. 12, 424–431. https://doi.org/10.1080/19336918.2018.1471322.
- Knooihuizen, S.A.I., Alexander, N.J., Hopke, A., Barros, N., Viens, A., Scherer, A., Atallah, N.J., Dagher, Z., Irimia, D., Chung, R.T., and Mansour, M.K. (2021). Loss of Coordinated Neutrophil Responses to the Human Fungal Pathogen, Candida albicans, in Patients With Cirrhosis. Hepatol. Commun. 5, 502–515. https://doi.org/10.1002/hep4.1645.
- Alexander, N.J., Bozym, D.J., Farmer, J.R., Parris, P., Viens, A., Atallah, N., Hopke, A., Scherer, A., Dagher, Z., Barros, N., et al. (2021). Neutrophil functional profiling and cytokine augmentation for patients with multiple recurrent infections: A case study. J. Allergy Clin. Immunol. Pract. 9, 986–988. https://doi.org/10.1016/j.jaip.2020.08.024.
- Barros, N., Alexander, N., Viens, A., Timmer, K., Atallah, N., Knooihuizen, S.A.I., Hopke, A., Scherer, A., Dagher, Z., Irimia, D., and Mansour, M.K. (2021). Cytokine Augmentation Reverses Transplant Recipient Neutrophil Dysfunction Against the Human Fungal Pathogen Candida albicans. J. Infect. Dis. 224, 894–902. https://doi.org/10.1093/infdis/jiab009.
- 84. Flamand, N., Boudreault, S., Picard, S., Austin, M., Surette, M.E., Plante, H., Krump, E., Vallée, M.J., Gilbert, C., Naccache, P., et al. (2000). Adenosine, a potent natural suppressor of arachidonic acid release and leukotriene biosynthesis in human neutrophils. Am. J. Respir. Crit. Care Med. 161, S88–S94. https://doi.org/10.1164/ajrccm.161.supplement_1. ltta-18.



STAR*METHODS

KEY RESOURCES TABLE

REAGENT or RESOURCE	SOURCE	IDENTIFIER
Chemicals, peptides, and recombinant proteins		
RPMI (w/o Phenol Red, L-Glutamate)	Gibco	11835030
1M HEPES	Gibco	15630080
Human Serum Albumin	Sigma	A5843
Hoechst 3334	Invitrogen	H3570
CalBryte 520 AM	AAT Bioquest	20650
Heat inactivated FBS	Gibco	16140-071
Poly-I-lysine	Sigma-Aldrich	P8920-100ml
ZETAG 8185	Solenic	N/A
Fibronectin from human plasma	Sigma	F0895
DPBS	Gibco	14190-144
BIIL315	Boehringer Ingelheim	N/A
Diphenyleneiodonium chloride (DPI)	MedChemExpress	HY-100965
Superoxide Dismutase from human erythrocytes	Sigma	9636-1KU
Catalase from human erythrocytes	Sigma	219008-1MG
Anhydrous DMSO	Invitrogen	D12345
Critical commercial assays		
Stemcell EasySep Direct Human Neutrophil Isolation Kit	StemCell Technologies	19666
Software and algorithms		
Fiji/ImageJ2 (v2.14.0/1.54f)	N/A	https://fiji.sc/
Python/Conda	N/A	https://anaconda.org/
ARCOS	N/A	https://arcos.gitbook.io/home/
Stardist	N/A	https://github.com/stardist/stardist
Julia	N/A	https://julialang.org/
Other		
.22um Seriflip Filter	Millipore Sigma	SE1M179M6
23-gauge butterfly needle collection set	BD	23-021-022
Vacutainer EDTA tubes	BD	366643
1.5H Glass Coverslip	Ibidi	10812
8-well sticky-Slide	Ibidi	80828
Fisherbrand LowRetention 1.5mL microcentrifuge tubes	Fisher	02681320

RESOURCE AVAILABILITY

Lead contact

Further information and requests for resources and reagents should be directed to and will be fulfilled by the lead contact, Orion Weiner (orion.weiner@ucsf.edu).

Materials availability

This study did not generate new reagents.

Data and code availability

- All data used in this work is available for free, open access download via Dryad at https://doi.org/10.5061/dryad.k0p2ngfg2.
- All code used in this work is available for free, open access download via Zenodo at https://doi.org/10.5281/zenodo.11123474.

Developmental Cell

Article



EXPERIMENTAL MODEL AND STUDY PARTICIPANT DETAILS

Healthy blood specimens from patients were obtained with informed consent according to the institutional review board-approved study protocol at the University of California - San Francisco (Study #21-35147). CGD blood specimens from patients were obtained with informed consent according to the institutional review board-approved study protocol at the Massachusetts General Hospital and the National Institutes of Health. Volunteers were informed not to take ibuprofen, acetaminophen, or more than one drink of alcohol within 24 hrs, class 1 or 2 antihistamines within 5 days, or aspirin within 7 days of blood draw. Volunteer demographics such as age and sex are provided in the final section of Methods S1. For most figures, the healthy UCSF donor pool was used. The NIH CGD and shipped control cohort was used to generate Figures 6E, 6F, S3B, and S3C (CGD), and Figures S6B, S6D, and S6E. Informed consent was obtained for use of human tissues in research.

METHOD DETAILS

Neutrophil Isolation Protocol

Imaging media was first prepared with RPMI (w/o Phenol Red, 25mM HEPES, L-Glutamate) and 0.4% Human Serum Albumin (HSA) (Sigma Cat: A5843). HSA was added directly to RPMI and then centrifuged at 500xg for 5 min until fully dissolved. The mix was then filtered with a $.22 \,\mu m$ Steriflip filter (Millipore Sigma: SE1M179M6) before further use. Imaging media was always prepared fresh on the same day of imaging.

Blood specimens from patients were obtained with informed consent according to the institutional review board-approved study protocol at the University of California - San Francisco (Study #21-35147). Fresh samples of peripheral blood (2 tubes, 7 mL each) from healthy adult volunteers were collected via a BD 23-gauge butterfly needle collection set (SKU: 23-021-022) into 10 ml BD Vacutainer EDTA tubes (SKU:366643). Volunteers were informed not to take ibuprofen, acetaminophen, or more than one drink of alcohol within 24 hrs, class 1 or 2 antihistamines within 5 days, or aspirin within 7 days of blood draw. Blood was kept on a shaker at minimum setting and utilized within 2 hours of the draw. Neutrophils were isolated using the Stemcell EasySep Direct Human Neutrophil Isolation Kit (#19666) with the BigEasy magnet (#18001) according to the manufacturer's protocol.

Isolated neutrophils were spun down at 200xg for 5 min and then resuspended in a dye media consisting of imaging media plus $5 \,\mu$ g/ml Hoechst 3334 (Invitrogen, Cat:H3570), and 1 μ M CalBryte 520 AM (AAT Bioquest, Cat: 20650). This cell suspension was incubated at room temperature in the dark for 15 min, and then spun down at 200xg for 5 min. The dye medium was aspirated and replaced with an amount of cell culture media of RPMI (Gibco) with 10% heat inactivated FBS (Gibco) needed to achieve a final cell density at or below $1x10^6$ cells/mL. Purified neutrophils were then kept in polystyrene T25 flasks at 37° C in a 5% CO2 environment until imaging. Cells were allowed to incubate for at least one hour before imaging began and not more than 5 hours after isolation. Allowing the cells to rest in culture before imaging helped ensure that Ca^{2+} signaling was more consistent and less noisy across volunteers.

CGD Cell Isolation

For CGD cells use in this work, the following changes to the above protocol were made. First, blood specimens were drawn from patients at the NIH campus for either control healthy donors or donors verified to have CGD. Samples were collected into 10ml BD Vacutainer EDTA tubes, and blood was shipped overnight in a temperature-controlled box using Phase 22 room temperature packs. Both CGD and healthy control blood were shipped together with each run to control for effects of shipping blood overnight to MGH. Blood was isolated in the same method as above as soon as it arrived in lab at around 10:30 am each day experiments were performed. Cells were not used more than 5 hours after isolation, and all accumulation experiments took place within 2 hours post isolation.

Neutrophil Swarming Chip Protocol

Swarming arrays of C. albicans were prepared as described previously, with modifications (6, 7). Briefly, we used a microprinting platform (Picospotter PolyPico Galway, Ireland) to print a solution of 0.1% poly-I-lysine (Sigma-Aldrich) with ZETAG 8185. For experiments, we printed arrays with either 1.0 mm or 1.5 mm spacing as indicated in an 8 well format on full sized No. 1.5H glass coverslips (Ibidi, Cat # 10812). Coverslips were dried and then left at room temperature until required. To attach an infection-like material to these arrays, 8-well sticky-Slide attachments (Ibidi, Cat # 80828) were overlaid on the printed arrays. An overnight culture of live C. albicans yeast was heat killed at 90° C for 20 minutes before being washed and re-suspended in dH2O, then $750 \, \mu$ L of this suspension was added to each well and incubated for 5 minutes. Following incubation, wells were thoroughly washed out with dH2O to remove unbound targets from the glass surface. Wells were screened to ensure appropriate patterning of targets onto the spots with minimal non-specific binding before use. The well attachment was then removed, and the coverslips were stored at 4° C until ready for use.

When preparing to use a patterned coverslip, the coverslip was first re-inspected for coating and target integrity. An Ibidi 8 well sticky-slide (Cat: 80828) was pressed firmly on to the slide, and a pipette tip was run along the bottom to ensure a proper seal was formed. The coverslip-well combo was then incubated in a 37° C oven overnight. Next a 200 μ L mixture of imaging media plus 15 μ g/ml Fibronectin from human plasma (Sigma, Cat: F0895) was pipetted into each well that was to be used that day. The slide was then incubated for 30 min at 37° C and washed 3x with 200 μ L/well of PBS (-/- Ca/Mg). The final wash of PBS was left on the well until imaging.



Developmental CellArticle

Neutrophil Swarming Imaging Protocol

Cells were imaged as follows except when using CGD cells (See below). Neutrophils in culture were taken and placed into Fisherbrand LowRetention 1.5mL microcentrifuge tubes (Cat: 02681320) and spun down at 200xg for 5 min. Cells were resuspended at variable concentrations ranging from $3x10^6$ - $10x10^6$ cells/mL in a freshly made solution of imaging media. These cell solutions were then allowed to rest at room temperature for 15 min. When the wait time had elapsed, the wash PBS was taken off the well to be imaged and $200~\mu$ L of the neutrophil solution pipetted into the well. Imaging began as soon as imaging conditions could be verified after placing the cells into the well. Most confocal microscopy data was collected using a Nikon Ti2-E body scope configured with a CrestOptics X-Light V2 confocal spinning disk system, a Lumencor Celesta light engine, Nikon 10x CFI Plan Apo Lambda objective, an Okobox temperature and CO_2 controlled environment, and a Photometrics Prime 95B sCMOS camera. Revision confocal microscopy data was collected using a Nikon Ti2-E body scope configured with a CrestOptics X-Light V3 confocal spinning disk system, a Lumencor Celesta light engine, Nikon 10x CFI Plan Apo Lambda objective, an Okobox temperature and CO_2 controlled environment, and a Photometrics Kinetix sCMOS camera. All data was taken using the same levels of laser power from the 405 nm and 488 nm. The camera was run in a 2x2 binning mode with a set exposure time of 200 ms for all channels. All videos are taken with a frame interval of 5 seconds between exposures unless otherwise indicated. All videos were taken at 37°C with 5% CO2 for the duration of imaging.

Where indicated, this protocol was modified as follows to add the inhibitors used in this study. For the LTB4 inhibitor BIIL315 (Boehringer Ingelheim via opnMe), the drug first resuspended in DMSO at a stock concentration of 10 mM. The stock was then diluted in resuspension media (RPMI+0.4%HSA) to a final concentration of 1 μ M before resuspending cells in the final step for imaging sample preparation. Cells were incubated in this drug-media solution for 15 min before starting the experiment. The drug was kept in solution for the duration of imaging. For Diphenyleneiodonium chloride, or DPI (MedChemExpress, Cat: HY-100965), the drug was bought in a premixed solution of DMSO at a stock concentration of 10 mM. The drug was diluted to a final concentration of 50 μ M in RPMI + 0.4% HSA before resuspending cells in the final step for imaging sample preparation. Cells were incubated in this drug-media solution for 15 min before starting the experiment. The drug was kept in solution for the duration of imaging. For SOD + Catalase, each lyophilized protein was separately suspended in imaging media (RPMI + 0.4% HSA) and allowed to dissolve. Aliquots were made and stored at -80C. Before imaging, aliquots were thawed on ice and diluted in imaging media to a final concentration of 200 U/mL for SOD (Sigma Cat #9636-1KU), >200U/mL for Catalase (Sigma Cat #219008-1MG). Since Catalase was provided with only a range of specific activity (>50,000 U/mL), the final concentration in the swarming assay was 4.27ug/mL to give an activity range of >213U/mL. Cells were incubated in this protein containing media solution for 15 min before starting the experiment. The proteins were kept in solution for the duration of imaging.

CGD Donor Cell Accumulation Imaging

Neutrophils in culture were taken and placed into 1.5 mL microcentrifuge tubes and spun down at 200xg for 5 min. Cells were resuspended at variable concentrations ranging from $3x10^6$ - $10x10^6$ cells/mL in a freshly made solution of imaging media. These cell solutions were then allowed to rest at room temperature for 15 min. When the wait time had elapsed, the wash PBS was taken off the well to be imaged and 200 μ L of the neutrophil solution placed in the well. End point accumulation imaging was performed 60 min after the wells were seeded with cells. Images were collected using a widefield florescence Nikon Ti-E body scope configured with a Nikon 10x Plan Flour objective equipped with a 37°C temperature and 5% CO2 environmental chamber.

CGD Donor Calcium Imaging

Neutrophils in culture were taken and placed into 1.5 mL microcentrifuge tubes and spun down at 200xg for 5 min. To avoid cell activation, cells were resuspended in the same media they were cultured in, RPMI + 10% FBS. These cells were left to rest for 15 min at room temperature, and then added to the well and imaged immediately. Timelapse imaging was performed on a Nikon Ti-E body widefield florescence scope, with a 10x Nikon objective, and wells were inside a stage top 37°C incubation unit.

Simulation Methods

In our study, we employed two distinct simulation approaches to model the system: a continuous partial differential equation (PDE) model and a discrete agent-based model.

Continuous PDE Simulation: For simulating the continuous PDE, we utilized the Julia Differential Equations package with the Rodas5P solver. This solver is a 5th order A-stable stiffly stable Rosenbrock method complemented by a stiff-aware 4th order interpolant. This choice was motivated by its robust performance in handling stiff equations when the step function is included. In the thick extracellular medium limit, we performed discretization in cylindrical coordinates (r, z), under the assumption of circular symmetry.

Discrete Agent-Based Simulation: The discrete agent-based model was simulated using the Julia CellBasedModels package. This method facilitates the modeling of interactions between cells and their medium. Unlike the continuous model, the stochastic nature of this approach breaks the circular symmetry. Therefore, we opted for a simpler ODE solver, the Tsit5 from the DifferentialEquations package. Tsit5, or the Tsitouras 5/4 Runge-Kutta method, offers a balance between accuracy and computational efficiency in the discrete model. Additionally, GPU computing significantly enhanced our simulation's performance of the large discrete simulations.

Developmental Cell

Article



QUANTIFICATION AND STATISTICAL ANALYSIS

Image Quantification

All image analysis presented in this work was achieved via the use of both Fiji (ImageJ) and Python. Images were pre-processed when needed to split one field of view into 4 quadrant ROIs to simplify the downstream Python analysis. All python analysis for each graph is provided as open-source code in the form of both scripts and Jupyter notebooks on Github (https://github.com/strickland-ev/swarming-self-extinguishing-relay-publication), and the same code is present on Zenodo https://doi.org/10.5281/zenodo. 11123474.

ARCOS Wave Tracking

See code posted on Github or Zenodo (https://doi.org/10.5281/zenodo.11123474) for a more direct explanation of the methods used and the code used for each figure. Broadly, to track cells trackpy was used to link frames where nuclei were identified via a custom StarDist model. The ARCOS algorithm was used to group like calcium events. Further analysis of cell tracks was done via custom python code included in the Github jupyter notebooks; the same code is also posted on Zenodo (https://doi.org/10.5281/zenodo.11123474).

Statistical Analysis

Details on each statistical analysis used in the figures are provided in the figure caption with the test details and test results. Briefly, a dependent paired t-test was used in Figure 1E, a Welch's t-test was used in Figure 2E, and a Welch's t-test was used in Figure 3G. Technical measurement number (n) and biological replicate number (N, independent volunteer samples) is always provided in the figure legend for each measurement given. Tests were performed with the standard python package scipy.stats. When averaging data over time in a figure, details are always provided in the figure legend. Data averages and confidence intervals are generated using the python seaborn package.